ATLAS Note

ATL-COM-MUON-2017-XX

Draft version 0.1

Design and Construction of the BIS 7/8 sMDT Chambers for the ATLAS Muon Spectrometer

O. Kortner[a], H. Kroha[a], S. Podkladkin[a], K. Schmidt-Sommerfeld[a], E. Takasugi[a]

[a]*Max-Planck-Institut fuer Physik, Munich*

24th May 2017

The construction and testing of new small-diameter Monitored Drift Tube (sMDT) BIS 7/8 chambers is presented.

Not reviewed, for internal circulation only

Contents

1 Introduction

The Monitored Drift Tube (MDT) chambers are one of four systems in the ATLAS Muon Spectrometer (see Fig. 1). The other systems are the Cathode Strip Chambers (CSCs), Thin Gap Chambers (TGCs), and Resistive Plate Chambers (RPCs). The MDT chambers have demonstrated that they provide very precise and robust tracking over large areas of the Muon Spectrometer. The Muon Spectrometer is designed to detect charged particles at pseudo-rapidities of $|\eta| \leq 2.7$ and accurately measure their momenta. More information about the Muon Spectrometer can be found in the ATLAS Muon TDR [1].

New chambers were constructed and tested to improve the rate capability of the MDT system, especially when the LHC luminosity is increased. These new chambers will also increase the precision of the muon momentum measurements and triggering. The small diameter Monitored Drift Tube (sMDT) chambers are one type of these new chambers designed for the higher-luminosity of future LHC operations. These new sMDT chambers consist of eight layers of pressurized drift tubes. These eight layers are split into two multilayers, positioned on either side of a spacer frame.

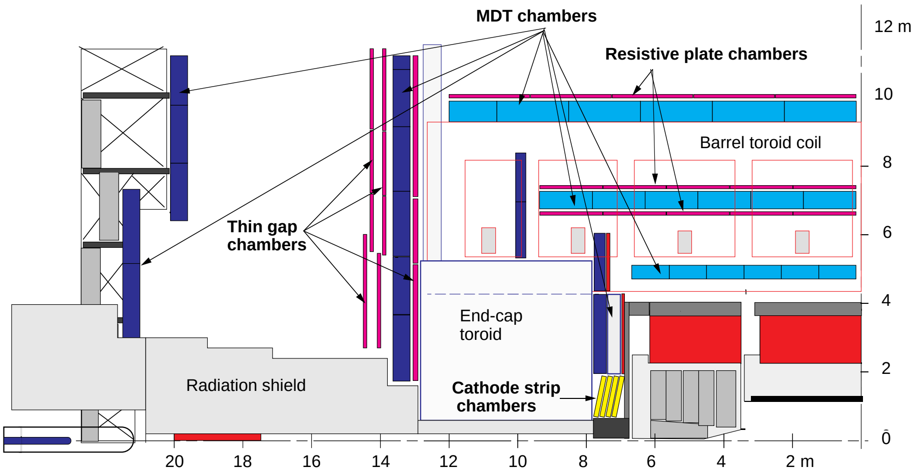

Figure 1: Quadrant view of the ATLAS Muon Spectrometer. The MDT chambers in the barrel (light blue) and in the endcap (dark blue) are in three layers. Figure from the ATLAS Muon TDR [1].

2 Monitored Drift Tube (MDT) Chambers

The MDT chambers are the main system for the ATLAS Muon Spectrometer's precision tracking system. They are precisely constructed and constantly monitored to quantify any deformations or changes in position during operation. The MDT chambers provide the primary momentum measurement in the Muon Spectrometer. They use pressurized drift tubes which are 30 mm in diameter and filled with Ar/CO_2 gas (with a 93:7 ratio), pressurized to 3 bar.

The MDT chambers are arranged into three layers in the barrel and three layers in both of the endcaps. The three layers in the barrel form coaxial cylinders around the beam axis, and the endcaps form circular disks all centered on the beam axis. The chambers in the innermost layer (both in the endcap and in the barrel) consist of eight layers of tubes, split into two equal multilayers, whereas the remaining chambers consist of six layers of tubes, also split into two equal multilayers. The chambers themselves are rectangular in

Table 1: MDT chamber parameters

Parameter	Design value
Tube diameter	30 mm
Wire diameter	50 μm
Gas mixture	Ar/CO_2 (93:7 ratio)
Gas pressure	3 bar (absolute)
Gas gain	2×10^4
Wire potential	3080 V
Average drift velocity	$\sim$ 20.7 μm/ns

the barrel region, but trapezoidal in the endcaps to create circular disks of MDT chambers. A table of the general MDT chamber parameters can be seen in Tab. 1.

A cross-section of one drift tube can be seen in Fig. 2. As a charged particle passes through the tube, the Ar/CO_2 gas is ionized. The electrons from the ionization clusters drift toward the anode wire. These drift velocities depend strongly on the radius, ranging from 10 μm/ns close to the tube wall, 26 μm/ns halfway between the wall and the wire, and 52 μm/ns close to the wire. These electrons create a sequence of pulses which are read out by the electronics seen in Fig. 3. More details about the MDT chamber electronics can be found in [2].

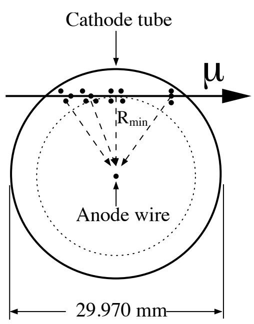

Figure 2: Cross section of a tube from an MDT chamber [2].

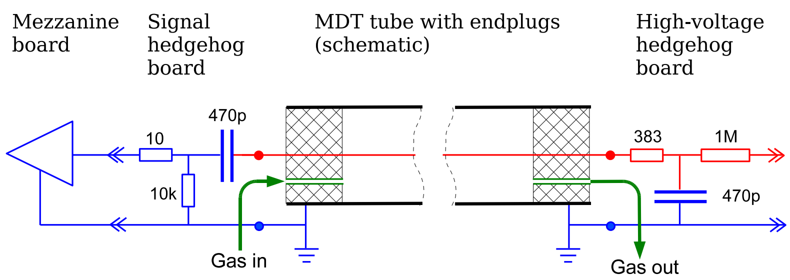

Figure 3: Schematic of a tube from an MDT chamber [2].

3 Small-Diameter Monitored Drift Tube (sMDT) Chambers

Small-diameter Monitored Drift Tube (sMDT) chambers utilize the same technology as the existing MDT chambers. However they differ in one major way: the tube diameter used is reduced by a factor of two in the sMDT chambers as opposed to the MDT chambers. This leads to a maximum drift time in the sMDT chambers which is almost one-fourth the time in a standard MDT chamber (see Fig. 6). This allows for an increase in rate capability of these new tubes of approximately one order of magnitude. Furthermore, the sMDT chambers themselves are geometrically smaller allowing them to be fitted into locations where standard MDT chambers are too large.

Table 2: MDT versus sMDT chamber parameters. The difference in HV ensures that the electric field inside the tubes, and therefore the gas gain, is identical in both types of chambers.

Parameter	MDT	sMDT
Diameter	30 mm	15 mm
Maximum drift time	700 ns	185 ns
Wire potential	3080 V	2730 V
Wire diameter	50 μm	
Gas mixture	Ar/CO_2 (93:7 ratio)	
Gas pressure	3 bar (absolute)	
Gas gain	2×10^4	
Chamber resolution	$\sim 40\ \mu$m	

The current production of sMDT chambers are designed to fit in the barrel region, next to the New Small Wheel (NSW) (see Fig. 4). These chambers will require “Cutouts” to prevent conflict with the NSW feet and support brackets (see Fig. 5). Thus, three differnet lengths of tubes are required. These different tube lengths also require a redesign of the construction process as the previous sMDT chambers all had equal-length tubes (BME and BMG chambers had only 2150 mm and 1120 mm tubes, respectively). There will be 12 BIS7/8 chambers in total.

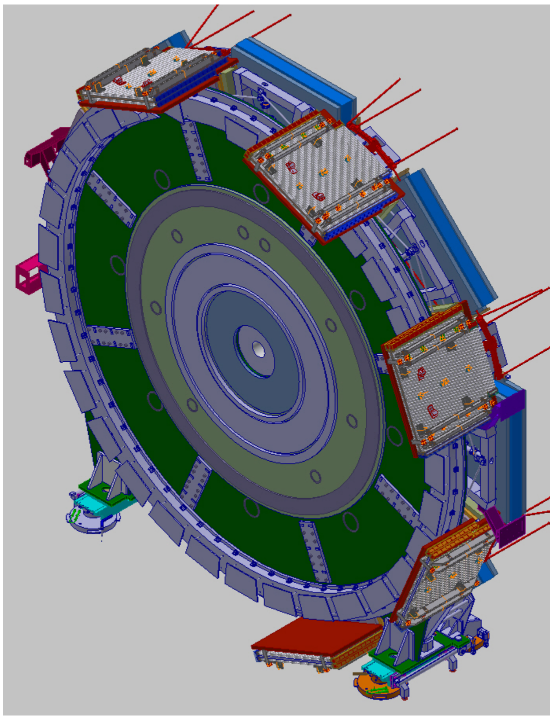

Figure 4: Location of the BIS7/8 chambers overlapping the NSW.

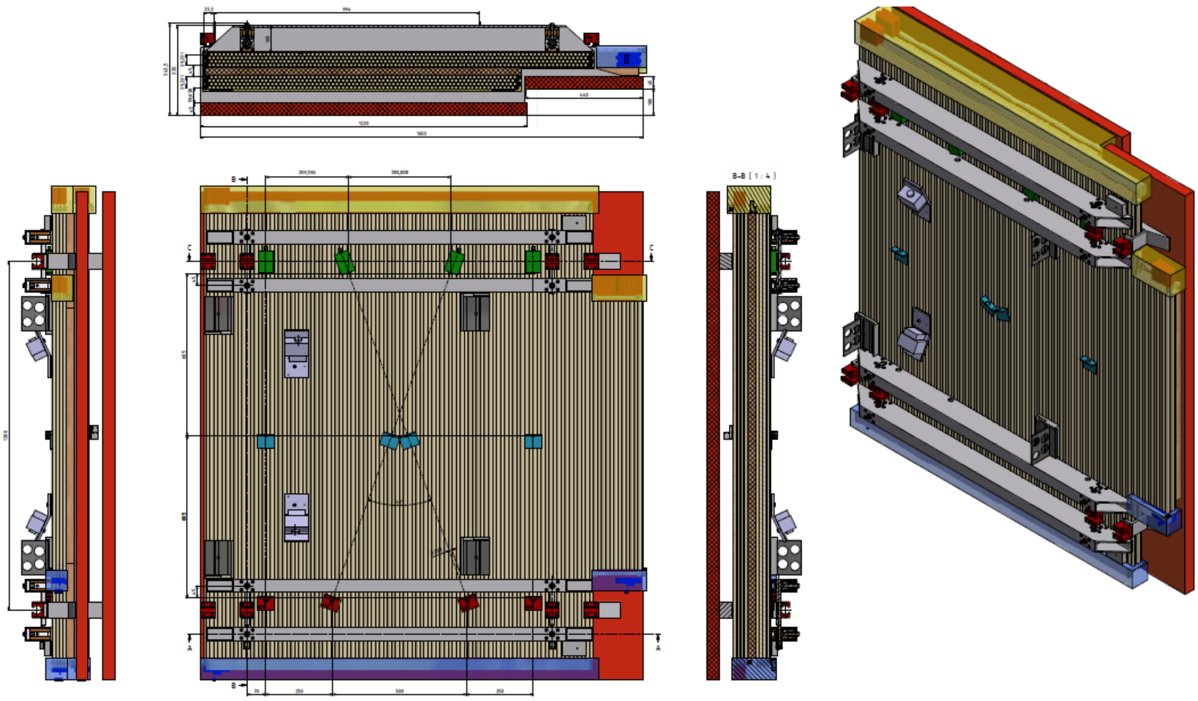

Figure 5: Image of a BIS7/8 from various angles. The cutouts required for the NSW can be seen in the centre bottom, top, and furthest right images.

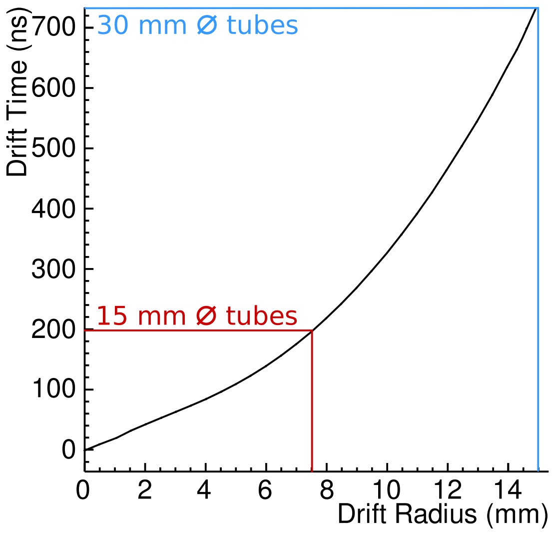

Figure 6: Maximum drift time versus tube radius. The old 30 mm tube drift time is noted in blue, whereas the new 15 mm tube drift time is noted in red.

4 sMDT BIS Chamber Construction

The sMDT BIS chamber construction takes place inside a clean room at MPI Munich. The tube lengths in the BIS chambers are 1660 mm, 1000 mm, and 1530 mm with a 15 mm diameter. Endplugs on either end cap the tube. Each tube is recorded in an MySQL database[3] along with the results from every test conducted on the tubes[1].

[1] The database can be found on the server at: http://134.107.29.19/ for current production, and http://134.107.29.19/tube_overview.php for BIS specific tubes. These pages are only accessible from within the MPI network.

5 sMDT Tube Construction and Testing

The tube construction starts with the threading of a Tungsten-Rhenium (W-Re) wire with 0.05 mm diameter semi-automatically into the tube using air pressure (see Fig. 8). The wire is then fastened to the first endplug with a copper tubelet. These endplugs not only hold the wire at the correct position ($\pm 5\ \mu$m) and tension, but also provide an airtight seal for the tube and enable HV supply and signal readout. An exploded view and cutaway of an endplug can be seen in Fig. 7.

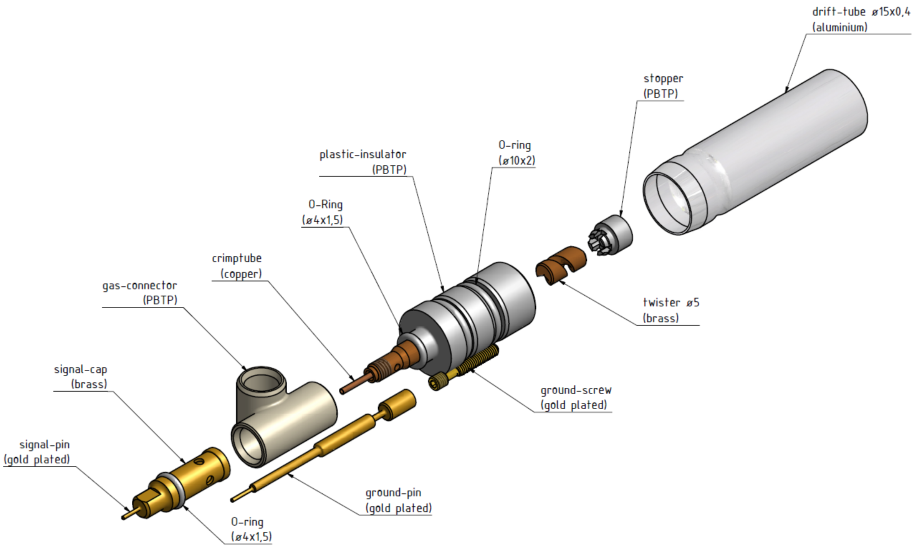

Figure 7: Exploded view of the tube endplug.

The first endplug is crimped into place and a second endplug is loosely placed into the other end of the tube. The wire is tensioned to 400 g for 10 seconds. This tension is removed, and the wire is re-tensioned to 350 ± 15 g. This tension is fixed with another copper tubelet on the other end, then the second endplug is crimped into place.

The wire tension is checked by applying a magnetic field to the wire, and passing an alternating current across the wire, which vibrates it. By noting the vibrational amplitude of the wire, the fundamental frequency of the wire can be found, which is directly related to the tension of the wire:

$$T = \frac{\pi L^2 d^2 f^2 \rho}{g} \tag{1}$$

where T is the tension, f is the frequency, d is the diameter of the wire, L is the length of the wire, and ρ is the density of the wire. Tab. 3 show the values used in the calculation. Furthermore, this measurement can be done without breaking the airtight seal on the tube endplugs and can be repeated multiple times (see Fig. 9). Multiple measurements are necessary as the wire relaxes in the tube over time, which leads to a decrease in the tension. On average, the tension decreases by approximately 5–10 g within the first few days (see Fig. 11) before stabilizing. The tubes are therefore checked for tension at least one week after the initial tensioning process to ensure that the wire tension remains within the specified range. These results are stored in the online MySQL database so they can be checked in real time.

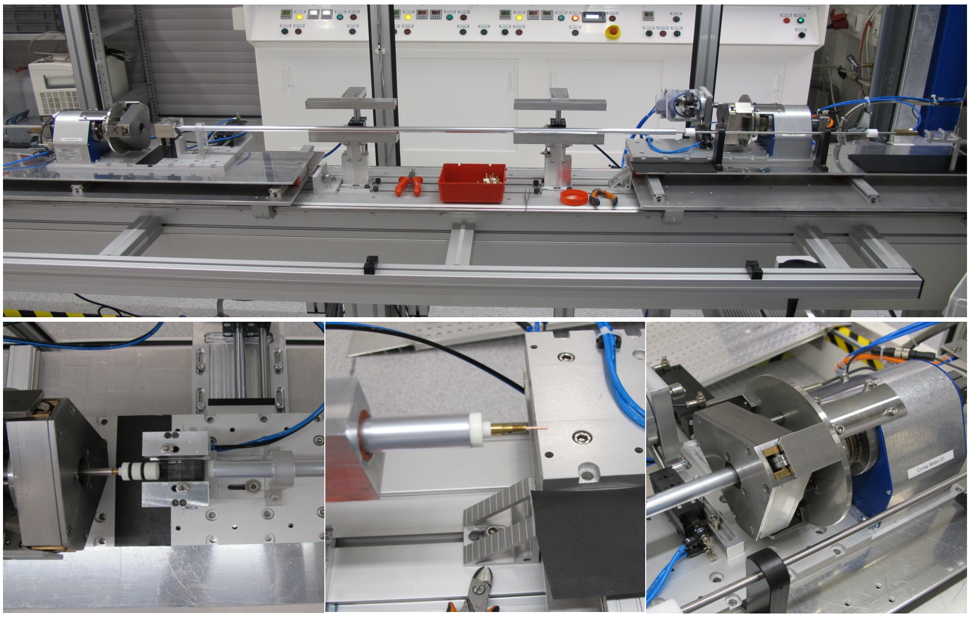

Figure 8: Wiring machine (top) with closeup of the endplug before insertion (bottom left), after insertion (bottom center), and component which allows for the threading of the wire (bottom right).

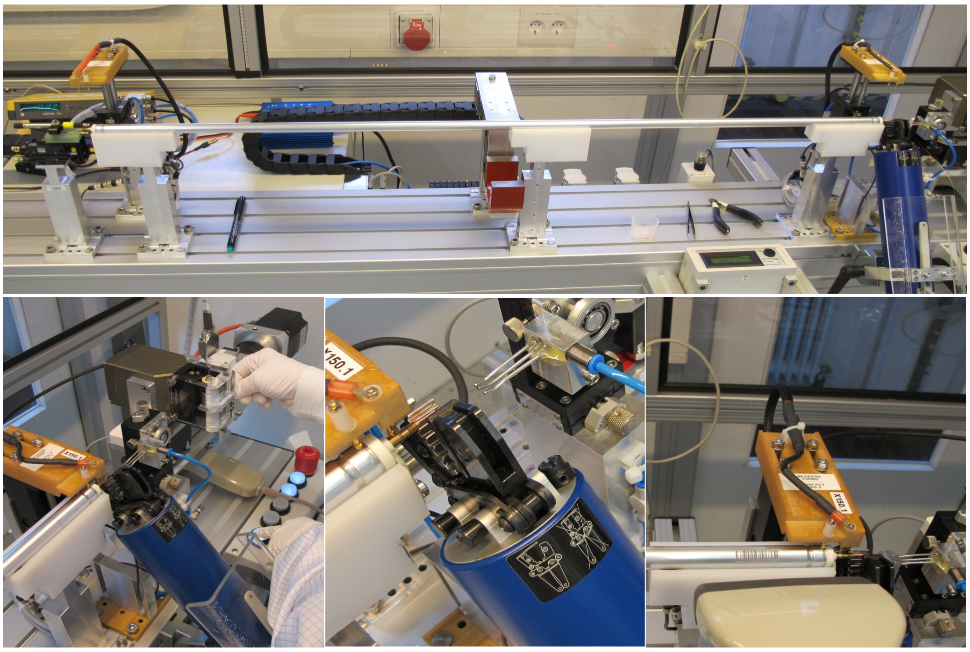

Figure 9: Wire tensioning machine (top), with a closeup of the tensioning device (bottom left), tube crimping (bottom center). The final step of entering the fundamental wire frequency and resistance into the database using the barcode associated with the tube (bottom right). The red component in the center of the top image is the magnet which, coupled with an alternating current, allows for an indirect measurement of the wire without opening the tube.

Constant	Value
L [mm]	1642, 982, or 1512
d [mm]	5×10^{-5}
ρ [g·cm^{-3}]	19.3
g [m/s^2]	9.81

Table 3: Wire parameters used in the calculation of the wire frequency using Eq. 1.

The results of the tension test are shown in Fig. 10. The tension limits (350 ± 15 g) are shown in dotted red lines. All passing tubes are colored green, while the failing tubes are colored red.

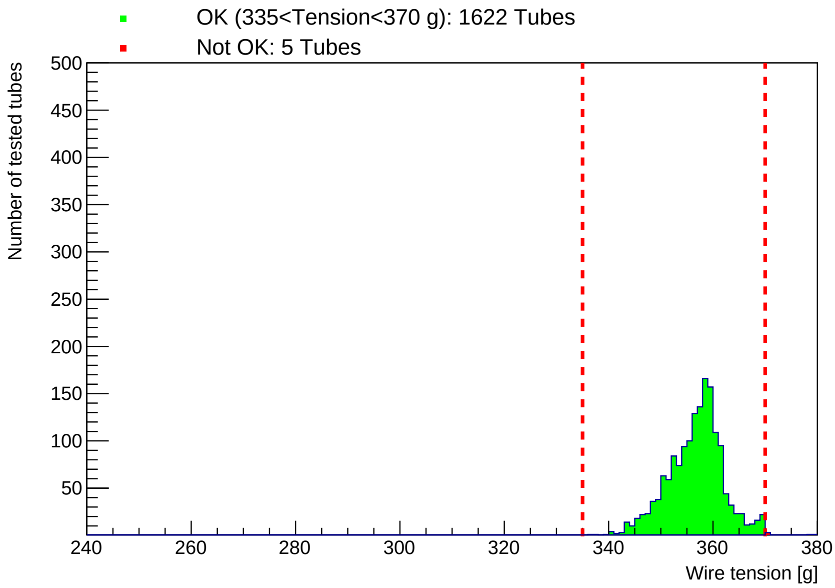

Figure 10: Tension measurements for all tested tubes. The required tension limits are shown in dotted red. The tubes which pass are in green, while the tubes which fail are in red.

After a second measurement is done (at least one week after the first test), the tension loss is recorded. Tubes which have a tension loss of more than 18 g are rejected. The change in tension is shown in Fig. 11. The majority of tubes are within the 5–10 g tension loss range, but there are some which have lost as much as 25–30 g of their tension. Not shown on the plots are those which have lost over 300 g tension, i.e., those whose wires have broken inside the tube due to either mishandling of the tube or a defect in the wire. The second tension measurement is required to be at least one week after the first test as after one week as the tension stabilizes after approximately seven days have passed. This was seen in the previous construction of sMDT tubes for the BMG chambers (Fig. 12).

Once the endplugs have been crimped, the gas seals are tested on the tube. The tubes are placed in an evacuated testing cylinder, which is also known as a "Torpedo". The sMDT tube is then filled with a mixture of 95% Ar, 5% He and pressurized to 2 bar. A leak detector, installed on the Torpedo, measures the amount of gas which escapes into the Torpedo from the tube. The measurement is then corrected for the difference between the gas mixture used and an all-argon gas. This leakage is required to be less than 10^{-5} mbar·l/s of argon. The leak rates are also recorded on the online MySQL database.

The results of the gas leak test can be seen in Fig. 14. As before, the red dotted line shows the acceptable leak

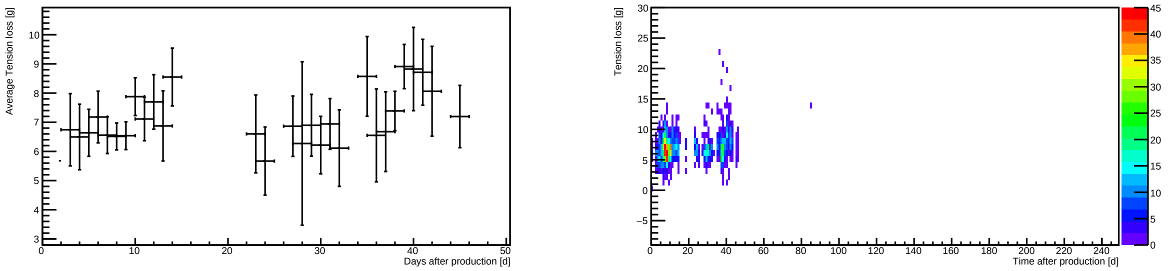

Figure 11: Average loss in tension (left) and the tension loss per tube (right) is shown as a function of time. On average, the tension decreases by approximately 5–10 g.

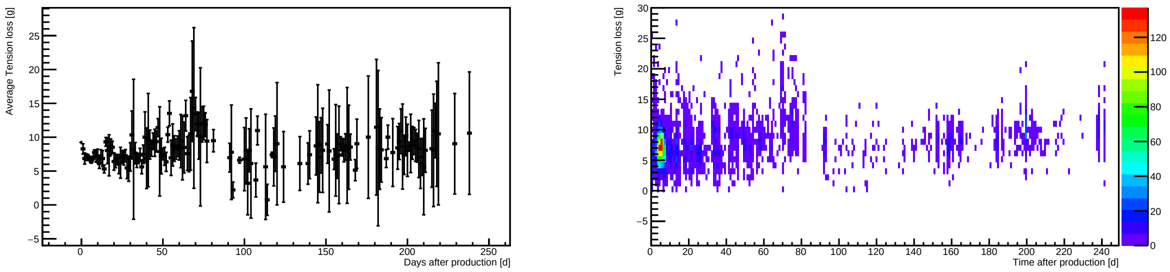

Figure 12: Average loss in tension (left) and the tension loss per tube (right) is shown as a function of time as seen in the BMG chambers. On average, the tension decreases by approximately 5–10 g. Figure from [4].

Figure 13: Gas leak testing. The central cylinder is the testing cylinder ("Torpedo"), which contains the tube. The lower left is the gas connection to the sMDT tube. The upper right leakage detector measures any gas which has leaked from the sMDT tube to the Torpedo.

rate limit of 10^{-5} mbar·l/s. The leak detection unit has a minimum detection sensitivity of 3×10^{-8} mbar·l/s, which is indicated by the dotted blue line. A large fraction of the tubes not only pass, but have a leak rate below the sensitivity of the detection unit, indicating that the construction and crimping process on the tubes is not only sound but reliably results in tubes which are in essence completely gas tight.

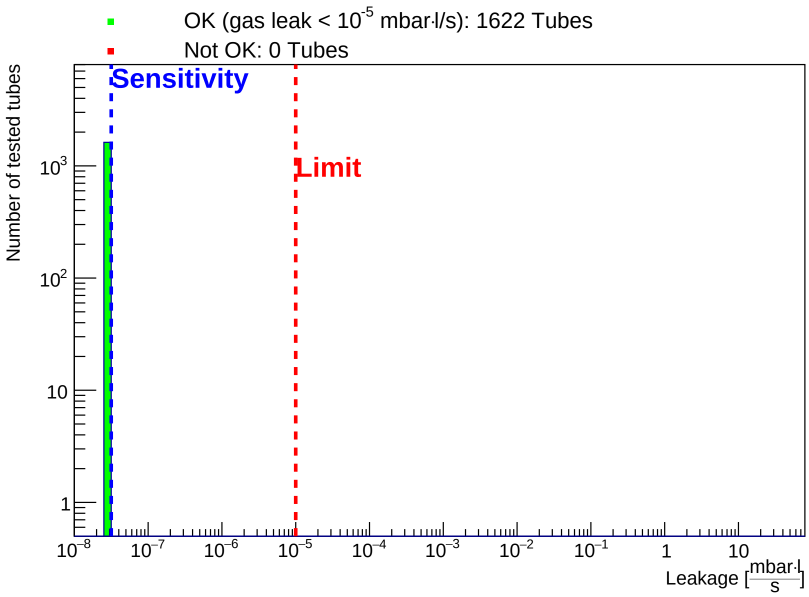

Figure 14: Measured gas leak rates for tubes. The limit (10^{-5} mbar·l/s) is shown in red, while the sensitivity of the leak detector (3×10^{-8} mbar·l/s) is shown in blue. The tubes which pass are in green, while the tubes which fail are in red.

After the gas seals have been tested, the sMDT tube is taken to HV testing. The tubes are filled with the nominal working gas (93% Ar, 7% CO_2) at 3 bar. The voltage is then slowly raised to 3,015 V, which is above the working voltage of 2,730 V. The dark current from the tube is continuously measured, and recorded after it stabilizes, which takes approximately 10 minutes. The measurement device (see Fig. 15) can test up to 15 tubes at a time, each with a separate HV source and current measurement device. The maximum allowed dark current is 2 nA per tube. Again, all results from the current test are recorded online in the MySQL database.

Figure 15: HV testing apparatus, shown with two tubes under test. This setup can test up to 15 tubes simultaneously.

The results of the HV test can be seen in Fig. 16. The limit of 2 nA is denoted by a dotted red line. The measurement device has a minimum sensitivity of 0.5 nA, which is shown by the dotted blue line. While most of the tubes are under the limit, there is a larger distribution of tubes which are above the allowed dark current. Not shown in the plots are those whose dark current is effectively infinite, i.e., the wire broke during transportation causing a short between the tube wall and the wire.

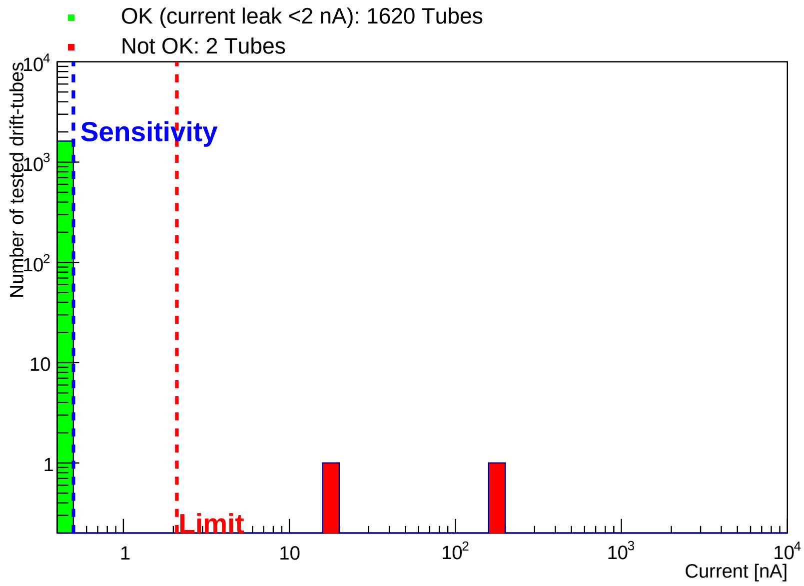

Figure 16: Measured dark current for tubes. The limit (2 nA) is shown in red, while the sensitivity of the dark current detector (0.5 nA) is shown in blue. The tubes which pass are in green, while the tubes which fail are in red.

During the course of the tube construction, other factors can disqualify a tube, including defects in the tube itself upon arrival, the breaking of the wire during handling, or a failure in the tubelets or endplugs. A chart showing the production losses can be seen in Fig. 17. The relative losses are enumerated in Tab. 4 and shown in Fig. 18. These tube statuses (if not directly related to the tests conducted on the tube) are also recorded in the MySQL database as a “Tube Status”. Their codes and meanings are listed in Tab. 5.

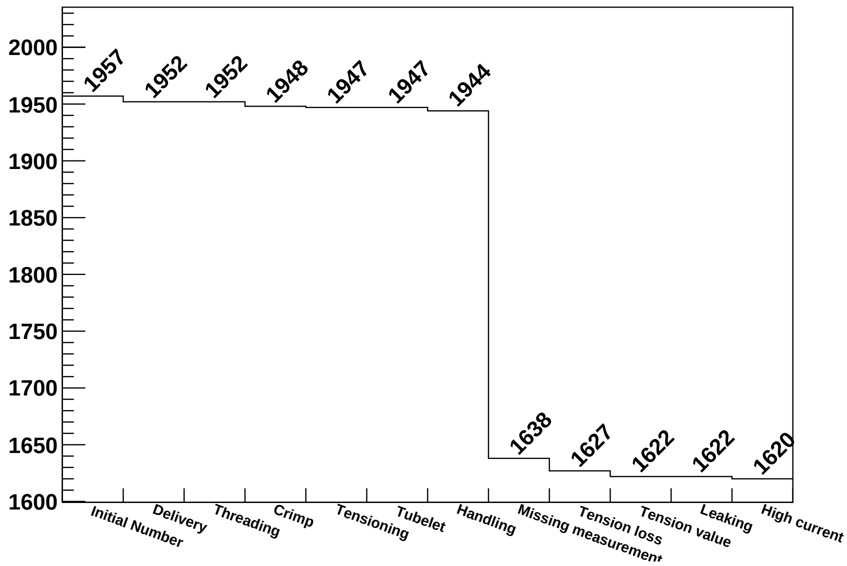

Figure 17: Tube production losses

Table 4: Tube production loss percentages

1957 Tubes	Total number
82.7798%	OK
0.102197%	High current
0%	Leaking
0.255493%	Tension value
0.562085%	Tension loss
15.6362%	Missing measurement
0.153296%	Handling
0%	Tubelet
0.0510986%	Tensioning
0.204394%	Crimp
0%	Threading
0.255493%	Delivery

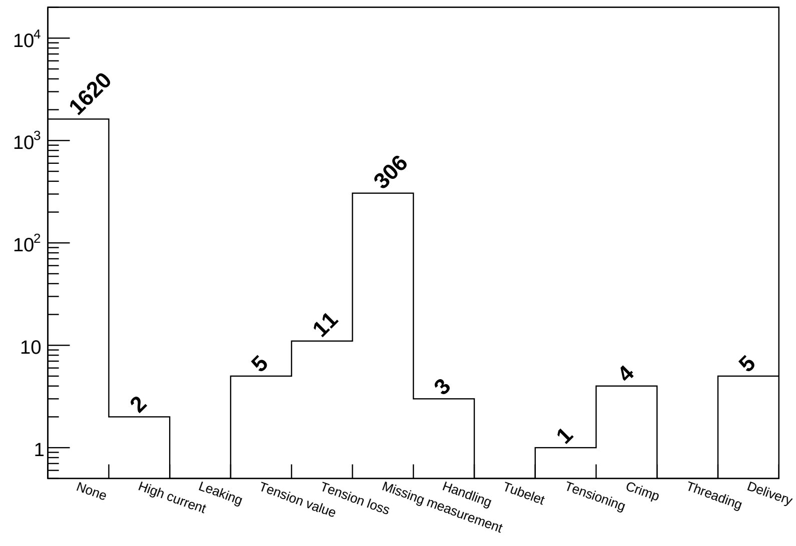

Figure 18: Tube production loss by category

Status Code	Meaning
0	OK
1	Dead On Arrival
10	Threading Error
11	Endplug Crimp Error
12	Tear During Tensioning
13	Crimp Tube Error
20	Tear During Handling

Table 5: Tube status and their meanings.

6 Chamber Construction

Once enough tubes for a chamber are produced, they are used to construct an sMDT chamber. Alignment combs (see Fig. 19) are used to ensure that the tubes, and more importantly the wires inside the tubes, are positioned in the proper place. This is crucial because the wires give the position readout of hits when a charged particle, i.e., a muon, passes through the tubes in a chamber. This is done by fixing the endplugs as closely as possible to a predetermined grid pattern. For each layer in the comb, there is a bottom half and top half which come together to encase and hold the tube endplugs in place. Because of the concentricity of the wire-and-endplug assembly, precise location of the endplug leads to precise positioning of the wires within the tube.

As these chambers use three different tube lengths, a series of combs had to be constructed. The first is for the most common tubes, with length 1660 mm. For the two different cutout lengths (100 mm and 1530 mm), two separate combs had to be made which could seamlessly be used in tandem with the 1660 mm tubes. Schematic of these combs can be seen in Figs. 20–22.

First, a layer of tubes is placed into the appropriate slots in the combs. As each tube is installed, their number is recorded in the MySQL database. After the first layer is in place, epoxy is laid down to prepare for the next layer of tubes (see Fig. 25). As each layer of tubes is placed, weights are used to ensure that the tubes stay in place as the glue cures (see Fig. 23). This process is repeated until the first multilayer (four layers' worth of tubes) is installed. An alignment frame and spacer are inserted, and the second multilayer is started. A schematic of the spacer and alignment frame can be seen in Fig. 24. After the second multilayer (again, with four layers' worth of tubes) is completed, the epoxy is left to set. Once the epoxy has set, the combs are removed from the chamber (see Fig. 26).

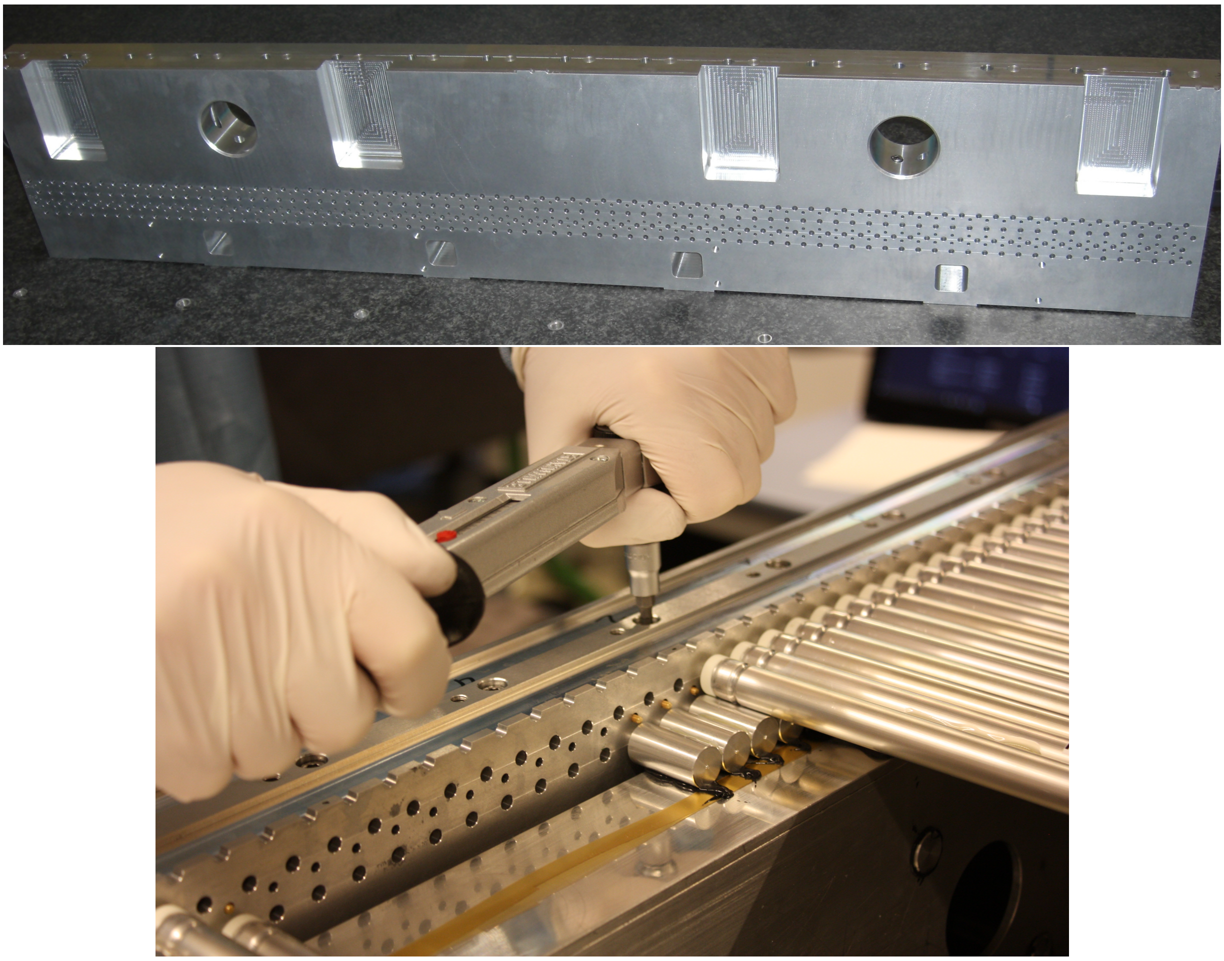

Figure 19: Alignment comb (top) used to align the tubes in each layer. The larger holes align the tubes, while the smaller holes guide the grounding contacts. Alignment comb in use with tubes installed (bottom).

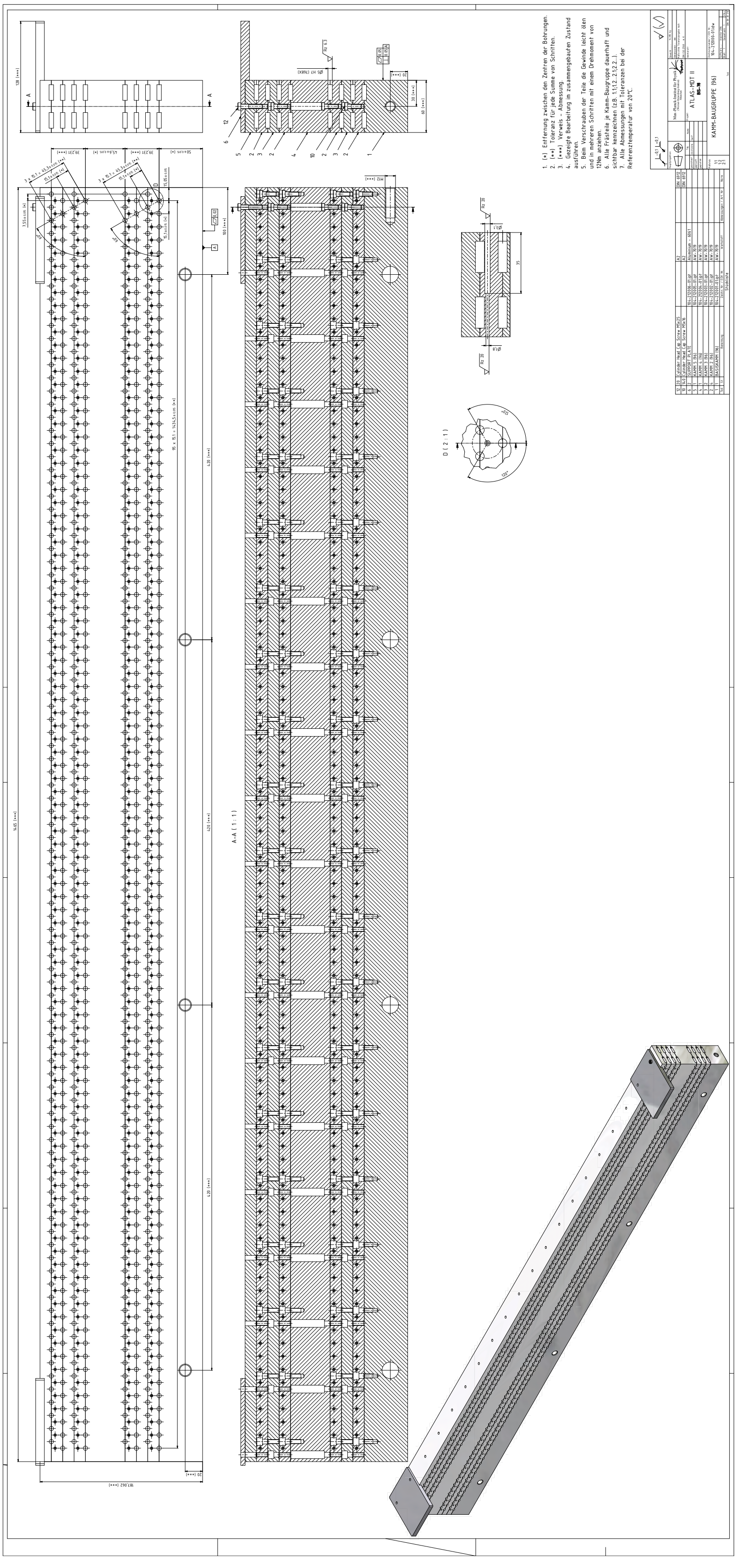

Figure 20: Schematic of longest the alignment comb. This runs almost the entire length of the BIS7/8 chamber

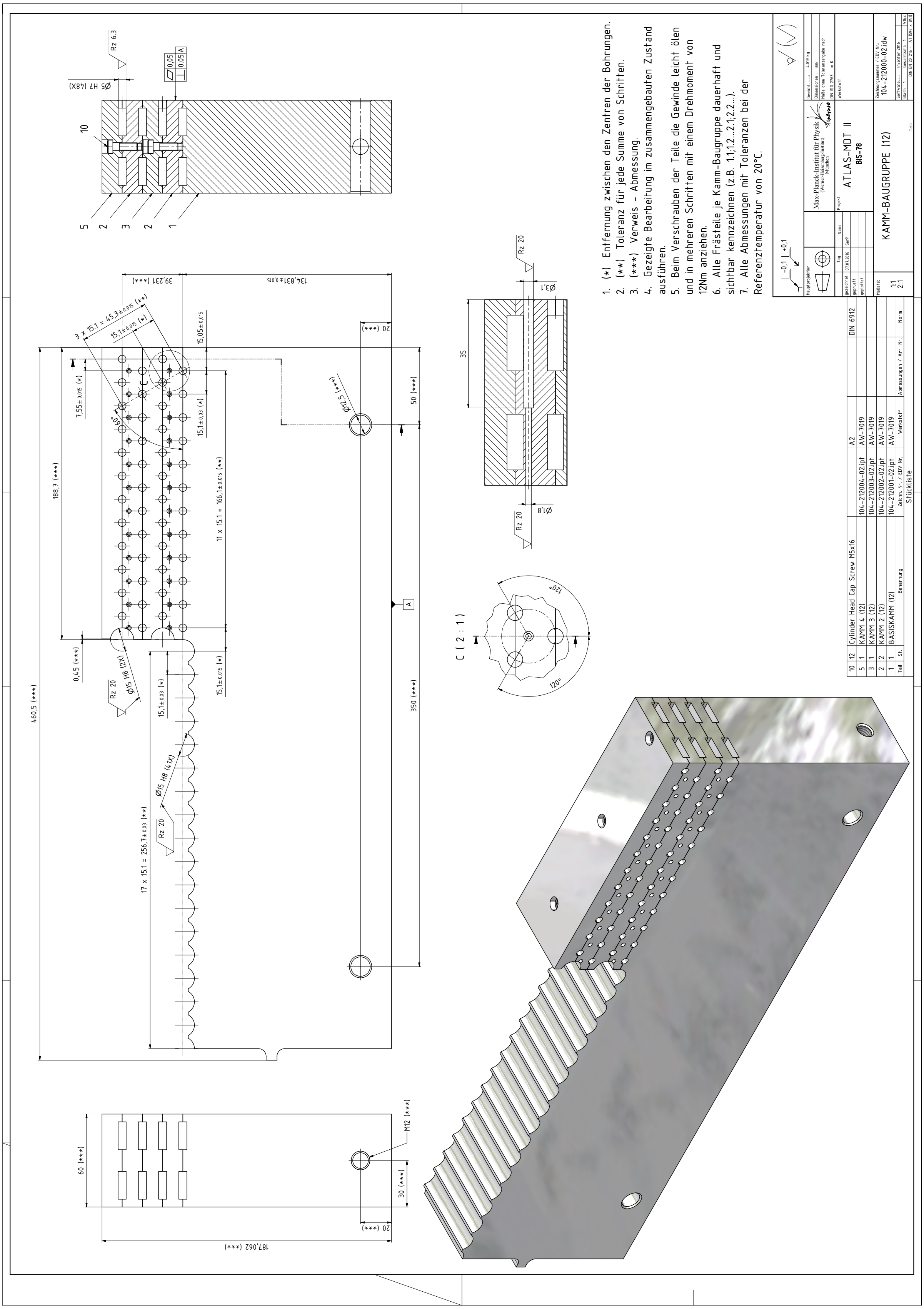

Figure 21: Schematic of the middle alignment comb. This allows for the 1530 mm tubes to be set into their proper place.

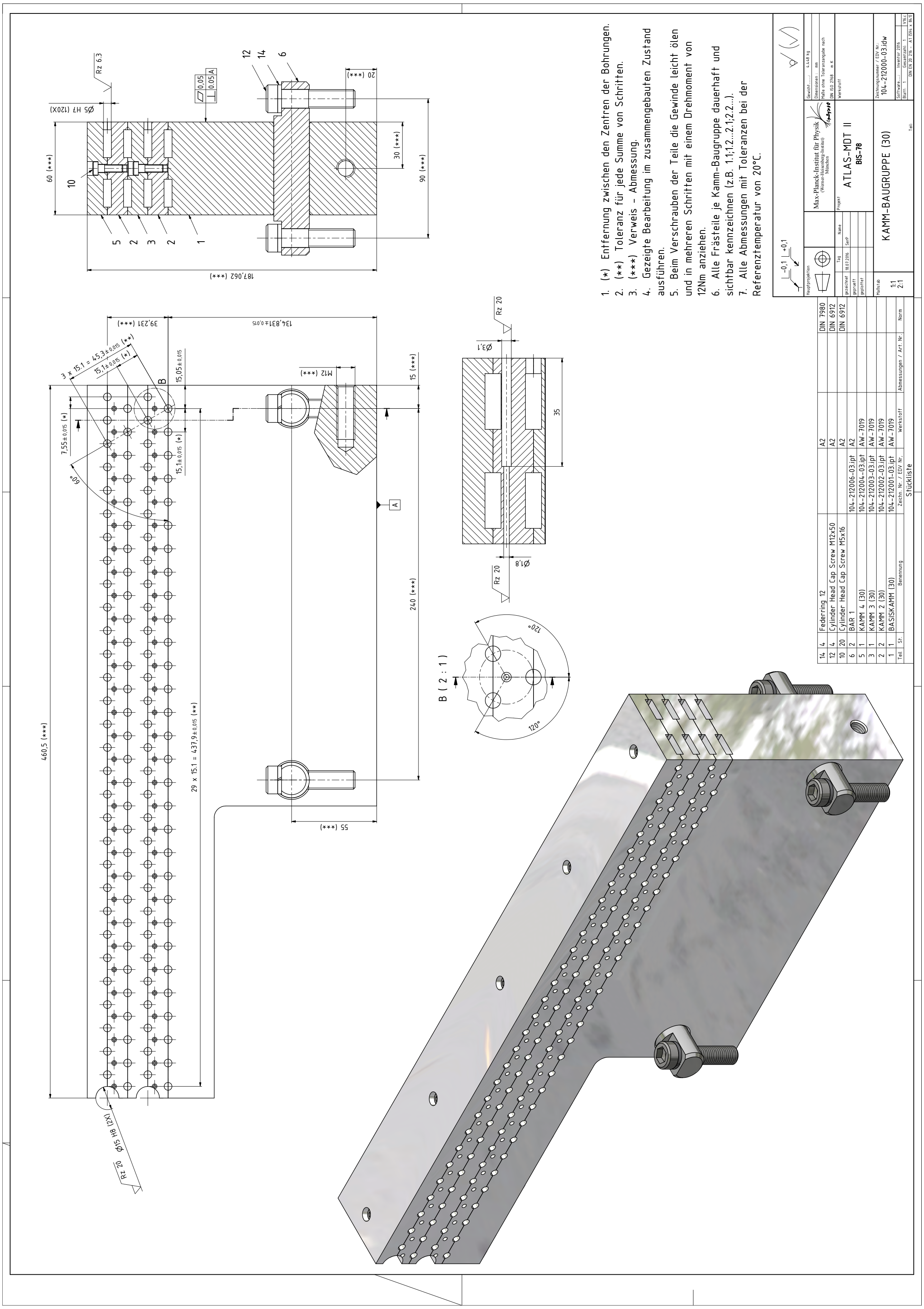

Figure 22: Schematic of the cutout alignment comb. This allows for the shortest 1000 mm tubes to be offset from the rest to allow for the NSW cutouts and feet.

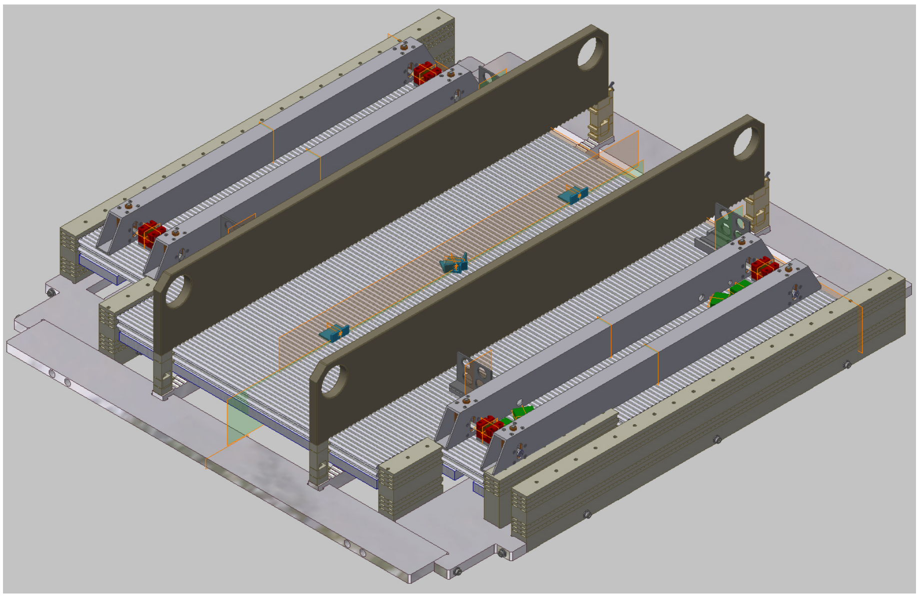

Figure 23: Image showing the weights used to keep the rubes in place as the epoxy cures. This is done after every layer of tubes is in place.

PLACEHOLDERPLACEHOLDER

Figure 24: Schematic of the spacer and alignment frame.

PLACEHOLDERPLACEHOLDER PLACEHOLDERPLACEHOLDER
PLACEHOLDERPLACEHOLDER PLACEHOLDERPLACEHOLDER

Figure 25: The first layer of tubes is set down using tube alignment combs (top left) and completed (top right). Epoxy is laid down to prepare for the second layer of tubes (bottom left) and the second layer is started (bottom right).

PLACEHOLDERPLACEHOLDER PLACEHOLDERPLACEHOLDER
PLACEHOLDERPLACEHOLDER PLACEHOLDERPLACEHOLDER

Figure 26: The alignment frame between the two multilayers is put in pace (top left) and the second multilayer is started (top right). The second multilayer is completed (bottom left). Once the epoxy has set, the combs are removed to show the completed chamber (bottom right).

7 sMDT BIS Chamber Testing

Once the tubes have been installed, the physical parameters of the chamber are measured and confirmed to ensure that the chamber's detection is within specifications. After a chamber is confirmed to be within specified parameters, the electronics are installed and tested as well.

7.1 Wire Position Measurement and Fitting

The concentricity between the wire and the tube endplug allows for a measurement of the wire position by measuring the position of the endplug for each tube (see Fig. 27). This is then fit to the ideal grid positions of the wires. The measurement is done on both sides of the chamber (the RO and HV side). Each side is fit separately first, then a combined fit is done to check for any overall torsion on the chamber. The results of these fits can be seen in Tab. 8, the torsion on the chambers can be seen in Tab. 9, and the residuals can be seen in Tab. 10.

Important to this is a measurement of the grid created by the combs as well in the placement of the wires. These were also run through the fit to confirm that each side was within specifications. The fitted comb parameters for the three different comb types can be seen in Tab. 6, and include the pitch in z, y, the size of the multilayer in y, the shift of the multilayer in z, and the RMS and σ of the z- and y-residuals. The RMS and σ of the z- and y-residuals of the fitted distributions are shown in Tab. 7.

The fitted chamber parameters (Tab. 8) include the pitch in z, y, the size of the multilayer in y, the shift of the multilayer in z, and the RMS and σ of the z- and y-residuals. Every chamber constructed is within nominal values. The RMS and σ of the z- and y-residuals of the fitted distributions are shown in Tab. 10. Overall, the RMS and σ of these decrease as more chambers were constructed. The residuals for a combined fit over all chambers is shown in Fig. 11. The torsion on each chamber (Tab. 9) are well below the tolerances of ATLAS, and are also below 0.5 milliradians.

PLACEHOLDER

Figure 27: Cutaway of tube endplug (left), and wire measurement using endplugs (right).

Table 6: Fitted comb parameters.

	12-hole Comb Measurement
z pitch [mm]	15.0996 ± 0.0001
y pitch [mm]	13.077 ± 0.0001
RMS (σ) z [mm]	0.0026 (0.0017)
RMS (σ) y [mm]	0.0027 (0.0019)
RMS (σ) r [mm]	0.0022 (0.0069)

	30-hole Comb Measurement
z pitch [mm]	15.0995 ± 0.00003
y pitch [mm]	13.0768 ± 0.0001
RMS (σ) z [mm]	0.0042 (0.0019)
RMS (σ) y [mm]	0.0071 (0.0076)
RMS (σ) r [mm]	0.0044 (0.0043)

	96-hole Comb Measurement
z pitch [mm]	15.0992 ± 0.00001
y pitch [mm]	13.0756 ± 0.000004
Multilayer Δz [mm]	0.006 ± 0.0002
Multilayer Δy [mm]	45.5978 ± 0.0005
RMS (σ) z [mm]	0.0054 (0.0049)
RMS (σ) y [mm]	0.0056 (0.0049)
RMS (σ) r [mm]	0.0056 (0.0052)

Table 7: Combined fitted comb position residuals in z, y, and $r = \sqrt{z^2 + y^2}$. N.B. The 12-hole comb had very small statistics causing the r-residual fit to look abnormal.

<table>
<tr><th></th><th>z-Residuals</th><th>y-Residuals</th><th>r-Residuals</th></tr>
<tr><td>12-hole Comb</td><td>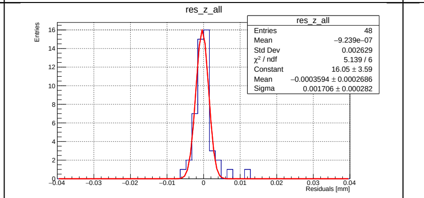
</td><td>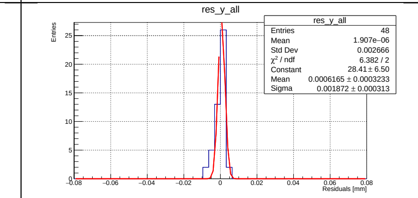
</td><td>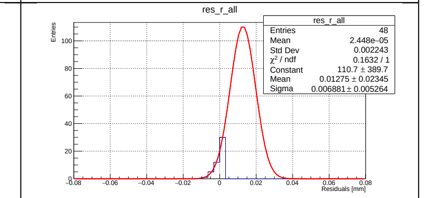
</td></tr>
<tr><td>30-hole Comb</td><td>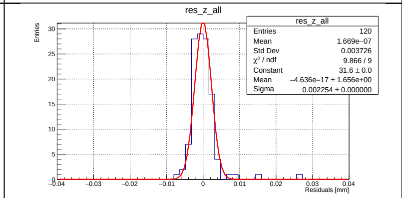
</td><td>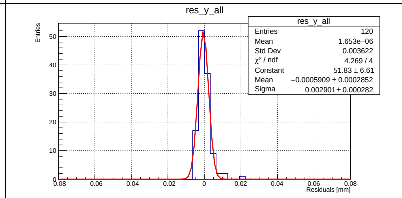
</td><td>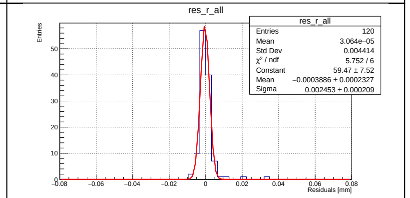
</td></tr>
<tr><td>96-hole Comb</td><td>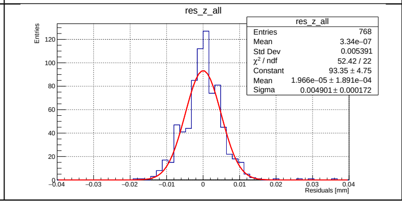
</td><td>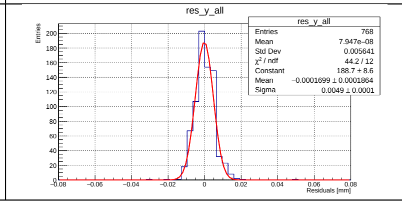
</td><td>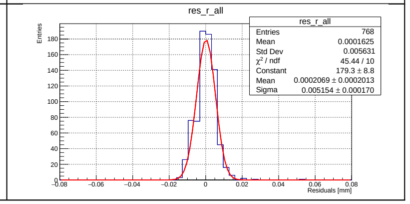
</td></tr>
</table>

Table 8: Fitted chamber parameters.

PLACEHOLDER	PLACEHOLDER	PLACEHOLDER	PLACEHOLDER	PLACEHOLDER

Table 9: Chamber torsion measurements, measure as the rotation of the HV side with respect to the RO side. Positive indicates a counter-clockwise rotation, as seen from RO side with the chamber in the upright position.

Chamber	RMS, r [μm]	σ r [μm]	Torsion [mrad]
PLACEHOLDER	PLACEHOLDER	PLACEHOLDER	PLACEHOLDER

Table 10: Fitted wire position residuals in z, y, and $r = \sqrt{z^2 + y^2}$.

Chamber	z-Residuals	y-Residuals	r-Residuals
PLACEHOLDER	PLACEHOLDER	PLACEHOLDER	PLACEHOLDER

Table 11: Combined fitted wire position residuals in z, y, and $r = \sqrt{z^2 + y^2}$.

HV/RO/Combined	z-Residuals	y-Residuals	r-Residuals
PLACEHOLDER	PLACEHOLDER	PLACEHOLDER	PLACEHOLDER

7.2 Gas, HV, and Electronics Installation

While the fits are done, the on-chamber electronics and gas systems are installed. This includes the high voltage connections to the wires, the electronics to read a signal from each tube and Faraday cages to reduce noise on the electronics. The basic schematic for the readout, HV, and gas system is similar to an MDT tube (see Fig. 3 for a basic schematic). For more details about the electronics boards, see [2].

The gas system is first installed, with inputs on the RO side and outputs on the HV side. The gas manifold runs across the width of the chamber, and distributes the gas in columns of four tubes per multilayer. Each multilayer has one pair of gas bars, one for input and one for output. On the RO side, gas is filled, while on the HV side, the gas is drawn out of the tubes. These are then connected to the input and output valves installed on the RO side of the chamber. A wire-frame of the gas system can be seen in Fig. 28. A cutaway of the gas distribution into four tubes can be seen in Fig. 41. The connection of one tube to the gas system can be seen in the lower left of Fig. 7.

Two boards are installed for the readout of the tubes on the RO side. First, a signal hedgehog board, which connects directly to the tubes, is installed. These boards read the signals from up to 24 tubes. Depending on the chamber, there are locations where these hedgehog boards are not installed. These correspond to the cutouts in the tubes for the ATLAS alignment system.

On top of the hedgehog board is an aluminum plate to reduce the noise seen from the chamber. A mezzanine board is installed above this, and connected directly to the hedgehog boards. These can read out the same number of tubes (24) as the hedgehog boards underneath. There are also mezzanine cards not installed which correspond to the cutouts in the chamber (see Fig. 44). These are connected to the CSM on the top of the chamber. The CSM provides communication between the chamber and the ATLAS system, providing the triggers to the chamber and delivering data from the chamber via optical fiber.

On the opposite (HV) side, the components for high voltage distribution are installed. The HV hedgehog cards, like the readout hedgehog boards, provide high voltage for up to 24 tubes. These are connected together via jumpers at five points: one for each of the four layers plus an additional for the ground. One card has an additional connection to the high voltage distribution box mounted on top of the chamber. The voltage distribution box takes two high voltage inputs, one for each multilayer, and distributes them, with one output cable per layer in the chamber and one last cable for ground.

Throughout the chamber, 14 temperature sensors are installed to ensure the chambers are at nominal temperature. These are connected to the MDT-DCS board on top of the chamber. This MDT-DCS board also takes input from the CSM (and thus from the mezzanine cards), providing parameters to the CSM and mezzanine cards for operation. The MDT-DCS board also provides for status and error monitoring of the CSM and mezzanine cards. Finally, Faraday cages are installed around the HV and RO electronics, and the boards on top of the chamber (CSM, DCS and HV distribution board) are also covered. A schematic of the Faraday cages can be seen in Fig. 42.

The completed chamber can be seen in Figs. 43–45. The physical parameters of the completed chambers can be seen in Tab. 12. The chamber is then run though the final set of tests.

Not reviewed, for internal circulation only

Table 12: Physical chamber parameters for all Side A BIS chambers.

Type	BIS78-A2	BIS78-A4/6	BIS78-A8/10	BIS78-A12	BIS78-A14	BIS78-A16
Radial distance from beam (mm)	4592	4550	4550	4550	4550	4635
Chamber width in z (mm)	1655	1655	1655	1655	1655	1655
Tubes width in z (mm)	1638	1638	1638	1638	1638	1638
Chamber length in x (mm), long	1839	1839	1839	1839	1839	1839
Chamber length in x (mm), cutout	1709	1709	1709	1709	1709	1709
Chamber length in x (mm), short	1179	1179	1179	1179	1179	1179
Aluminum tube length (mm), long	1660	1660	1660	1630	1630	1660
Assembled tube length (mm), long	1669	1669	1669	1639	1639	1669
Aluminum tube length (mm), cutout	1530			1530	1530	1530
Assembled tube length (mm), cutout	1539			1539	1539	1539
Aluminum tube length (mm), short	1000	1000	1000	1000	1000	1000
Assembled tube length (mm), short	1009	1009	1009	1009	1009	1009
Tube layers, long/cutout	2×4	2×4	2×4	2×4	2×4	2×4
Tube layers, short/cutout	4	4	4	4	4	4
Tubes/layer, long, ML1	78	78	66	66	66	66
Tubes/layer, long, ML2	66	96	84	54	54	54
Tubes/layer, cutout, ML2	30			30	30	30
Tubes/layer, short, ML2	12	12	12	12	12	12
Tubes/layer, ML1	78	78	65	66	66	66
Tubes/layer, ML2	108	108	96	96	96	96
Tubes/chamber, long	576	696	600	480	480	480
Tubes/chamber, cutout	120			120	120	120
Tubes/chamber, short	48	48	48	48	48	48
Tubes/chamber	744	744	648	648	648	648
Spacer height (mm)	45.6	45.6	45.6	45.6	45.6	45.6
Tubes height (mm)	139	139	139	139	139	139
Chamber height (mm)	249	249	249	249	249	249
Gas volume/chamber (l)	188.1	190.6	165.3	160.6	160.6	162.9
Chamber weight (kg)	170	170	150	150	150	150
Mezz. cards (24 ch.)/chamber	31	31	27	27	27	27
Mezz. cards/CSM 1 (inner ML1)	13	13	11	11	11	11
Mezz. cards/CSM 2 (outer ML2)	18	18	16	16	16	16
Temperature sensors/chamber	16	16	16	16	16	16
Magnetic field sensors/chamber	2	2	2	2	2	2
Praxial alignment platforms	8	8	8	8	8	8
Survey targets	4	4	4	4	4	4

Table 13: Physical chamber parameters for all Side C BIS chambers.

Type	BIS78-C2	BIS78-C4/6	BIS78-C8/10	BIS78-C12	BIS78-C14	BIS78-C16
Radial distance from beam (mm)	4635	4550	4550	4550	4550	4635
Chamber width in z (mm)	1655	1655	1655	1655	1655	1655
Tubes width in z (mm)	1638	1638	1638	1638	1638	1638
Chamber length in x (mm), long	1839	1839	1839	1839	1839	1839
Chamber length in x (mm), cutout	1709	1709	1709	1709	1709	1709
Chamber length in x (mm), short	1179	1179	1179	1179	1179	1179
Aluminum tube length (mm), long	1660	1660	1660	1630	1630	1660
Assembled tube length (mm), long	1669	1669	1669	1639	1639	1669
Aluminum tube length (mm), cutout	1530			1530	1530	1530
Assembled tube length (mm), cutout	1539			1539	1539	1539
Aluminum tube length (mm), short	1000	1000	1000	1000	1000	1000
Assembled tube length (mm), short	1009	1009	1009	1009	1009	1009
Tube layers, long/cutout	2×4	2×4	2×4	2×4	2×4	2×4
Tube layers, short/cutout	4	4	4	4	4	4
Tubes/layer, long, ML1	78	78	66	66	66	66
Tubes/layer, long, ML2	66	96	84	54	54	54
Tubes/layer, cutout, ML2	30			30	30	30
Tubes/layer, short, ML2	12	12	12	12	12	12
Tubes/layer, ML1	78	78	66	66	66	66
Tubes/layer, ML2	108	108	96	96	96	96
Tubes/chamber, long	576	696	600	480	480	480
Tubes/chamber, cutout	120			120	120	120
Tubes/chamber, short	48	48	48	48	48	48
Tubes/chamber	744	744	648	648	648	648
Spacer height (mm)	45.6	45.6	45.6	45.6	45.6	45.6
Tubes height (mm)	139	139	139	139	139	139
Chamber height (mm)	249	249	249	249	249	249
Gas volume/chamber (l)	188.1	190.6	165.3	160.6	160.6	162.9
Chamber weight (kg)	170	170	150	150	150	150
Mezz. cards (24 ch.)/chamber	31	31	27	27	27	27
Mezz. cards/CSM 1 (inner ML1)	13	13	11	11	11	11
Mezz. cards/CSM 2 (outer ML2)	18	18	16	16	16	16
Temperature sensors/chamber	16	16	16	16	16	16
Magnetic field sensors/chamber	2	2	2	2	2	2
Praxial alignment platforms	8	8	8	8	8	8
Survey targets	4	4	4	4	4	4

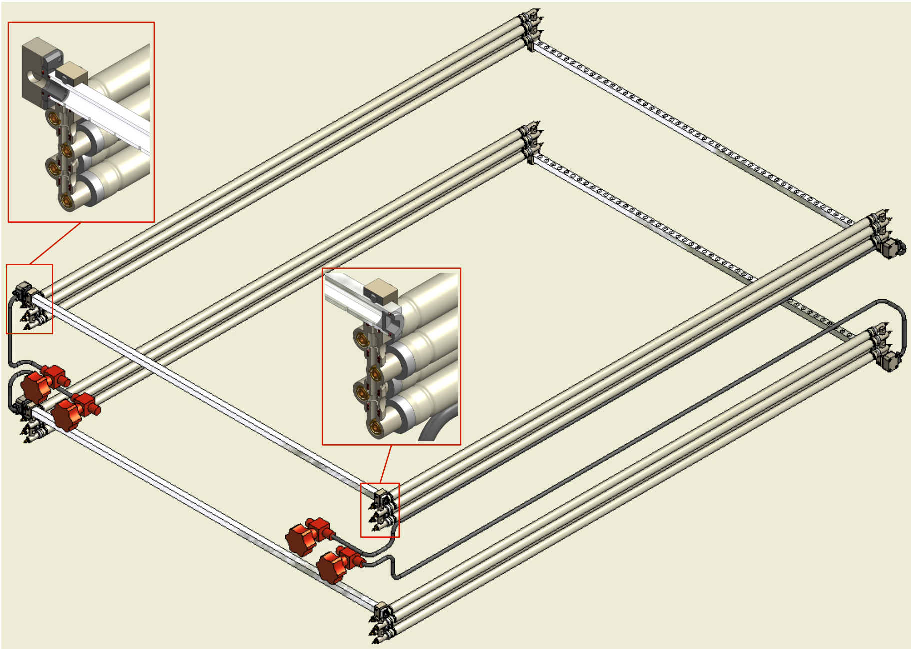

Figure 28: A wire-frame view of the gas system on the BMG chambers. Inset are closeups of the distribution of the gas over a vertical column of four tubes on the RO side. A similar setup is on the HV is used to consolidate the gas outputs in each multilayer.

Table 14: Physical chamber parameters for BIS 1-6 chambers (* refer to sectors 2 and 16).

Type	BIS 1	BIS 2-6
Number of chambers	80	16
Radial distance from beam (mm)	4550 (4635)*	4550 (4635)*
Chamber width in z (mm)	1113	933
Tubes width in z (mm)	1096	916
Chamber length in x (mm)	1839	1839
Aluminum tube length (mm)	1660	1660
Assembled tube length (mm)	1669	1669
Tube layers	2×4	2×4
Tubes/layer	72	60
Tubes/chamber	576	480
Spacer height (mm)	45.6	45.6
Tubes height (mm)	139	139
Chamber height (mm)	249	249
Gas volume/chamber (l)	151	126
Chamber weight (kg)	100	86
Mezz. cards (24 ch.)/chamber	24	20
Mezz. cards/CSM 1 (inner ML1)	12	10
Mezz. cards/CSM 2 (outer ML2)	12	10
Temperature sensors/chamber	10	10
Magnetic field sensors/chamber	2	2
Praxial alignment platforms	4	4
Survey targets	4	4

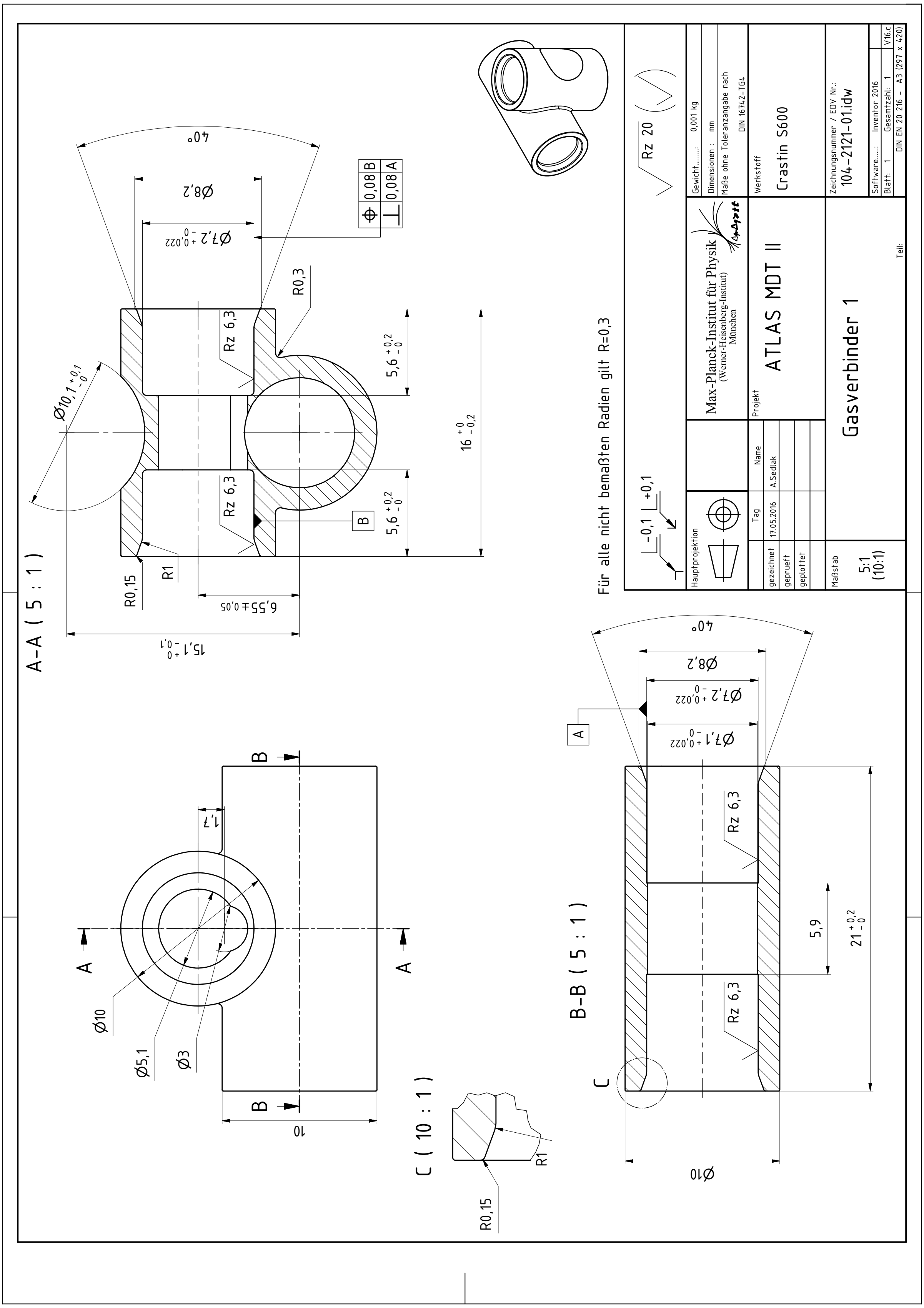

Figure 29: Schematic of first of eight gas distribution components stacked in groups of four to connect four tubes to gas.

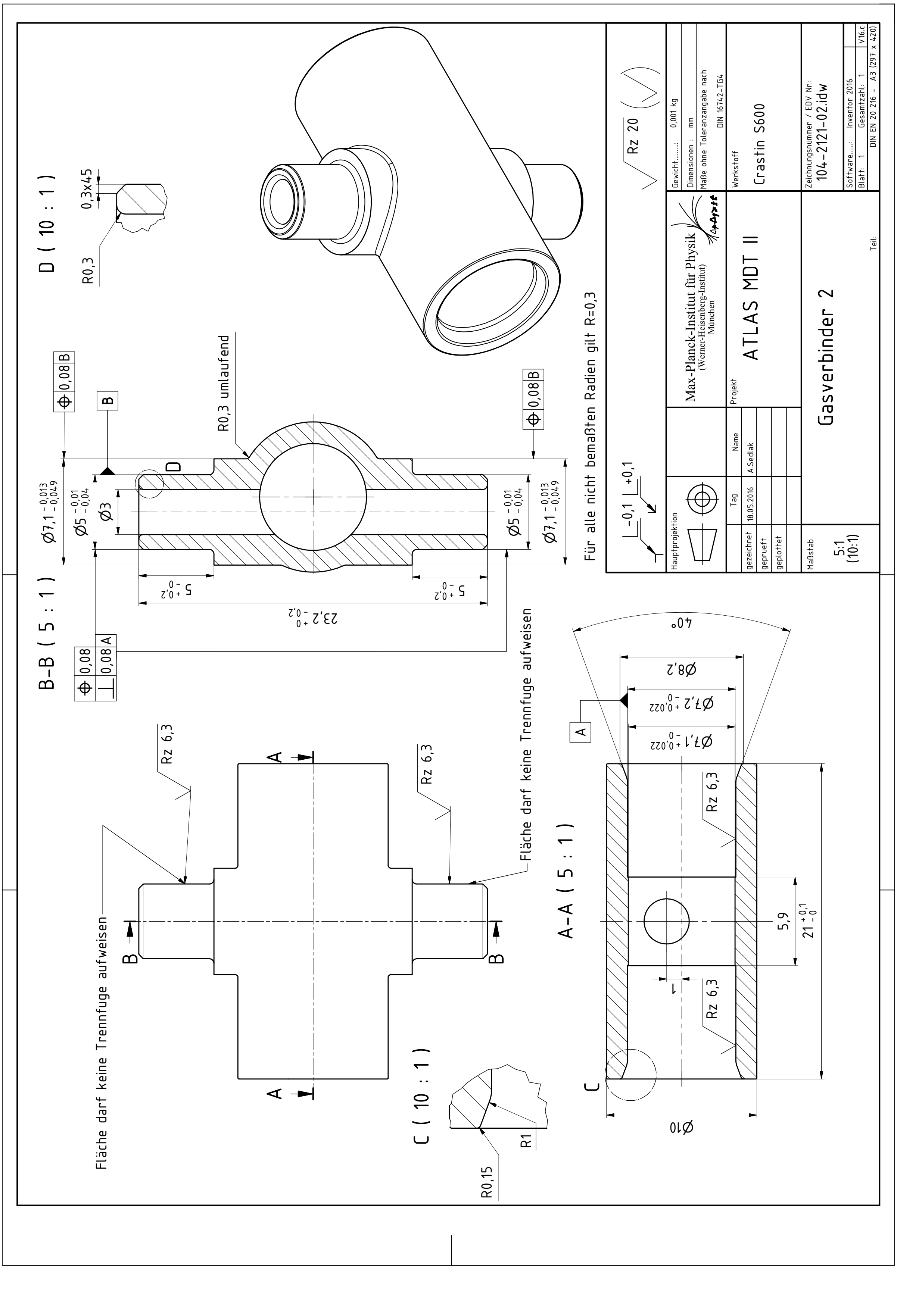

Figure 30: Schematic of second of eight gas distribution components stacked in groups of four to connect four tubes to gas.

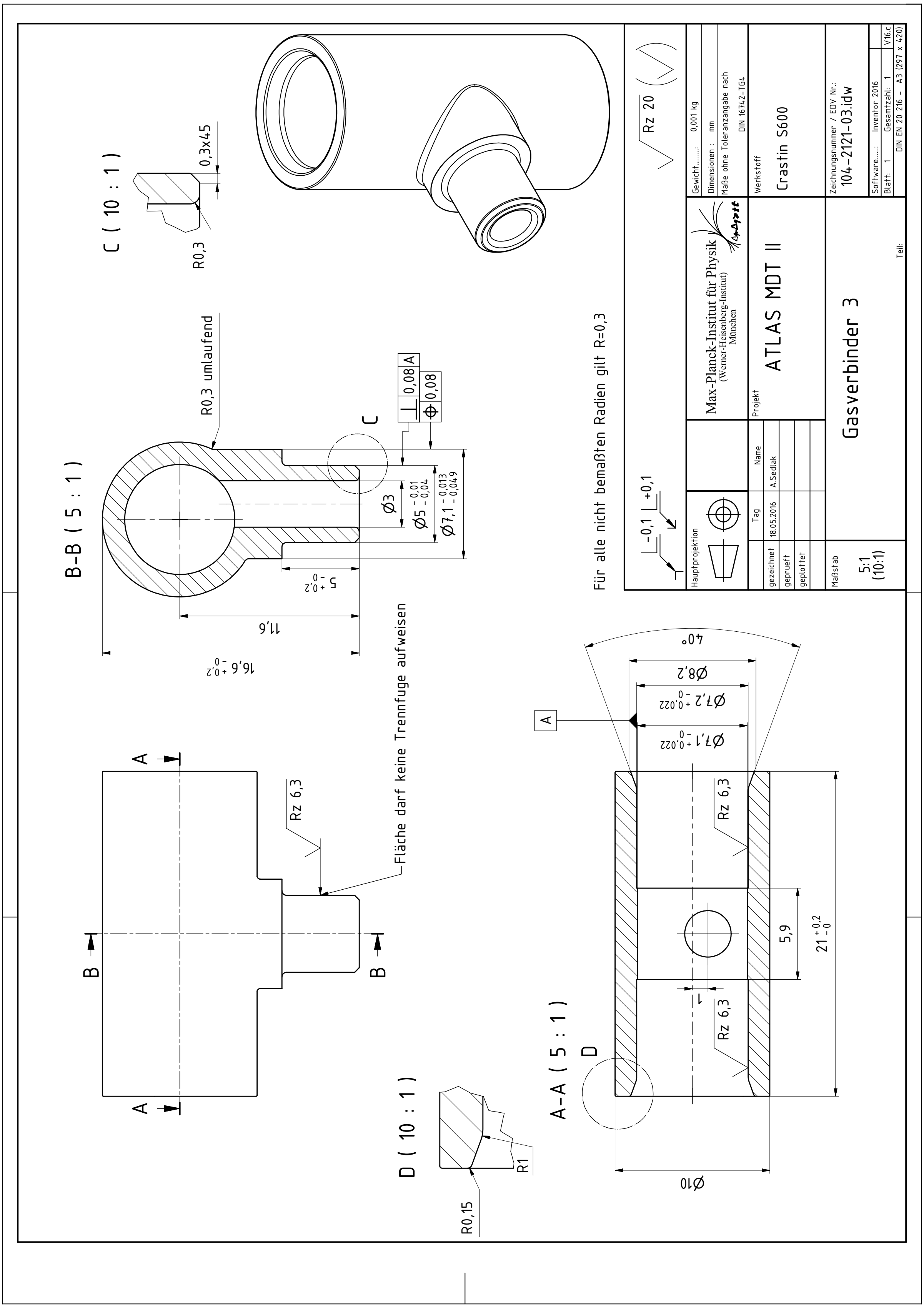

Figure 31: Schematic of third of eight gas distribution components stacked in groups of four to connect four tubes to gas.

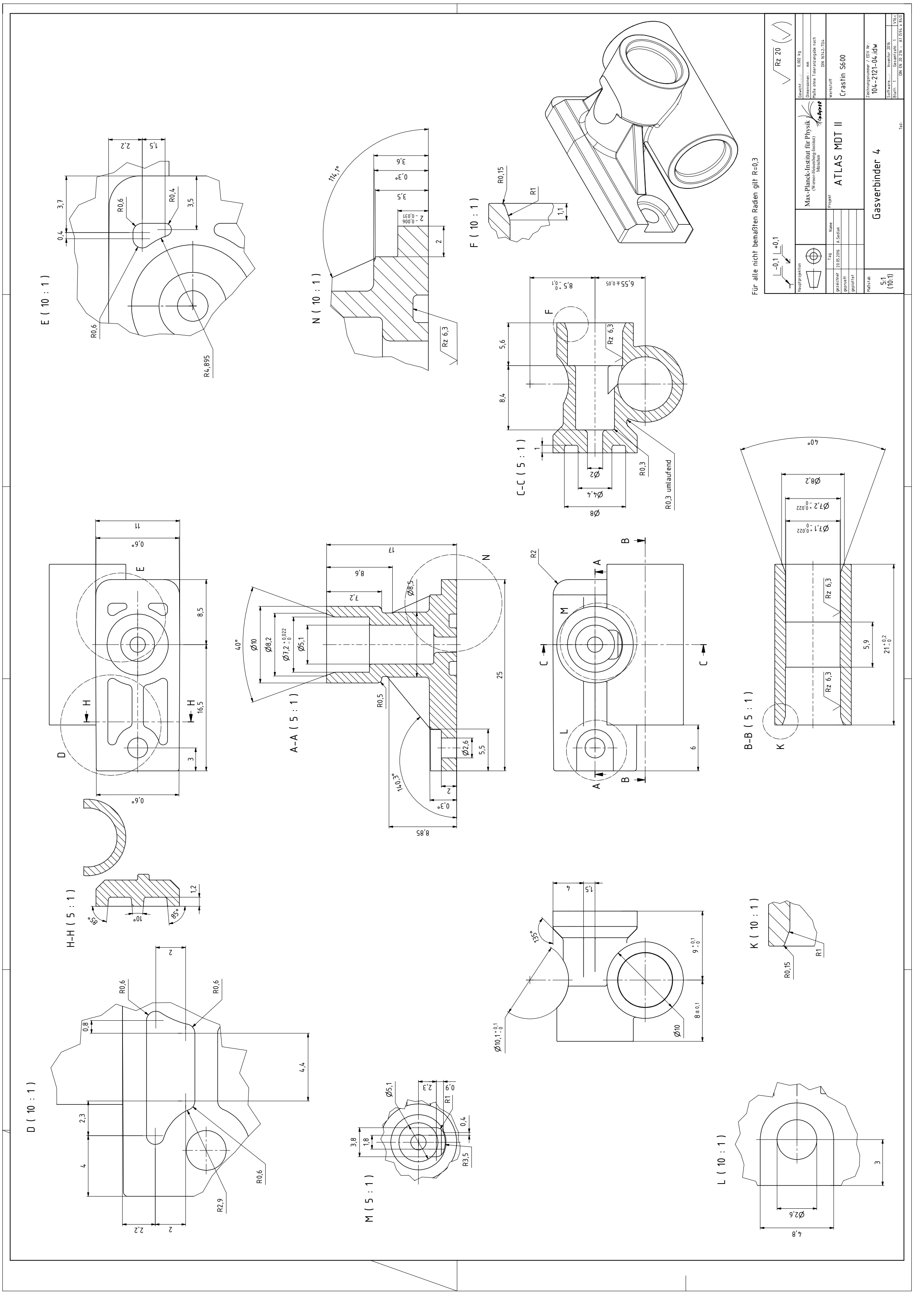

Figure 32: Schematic of fourth of eight gas distribution components stacked in groups of four to connect four tubes to gas.

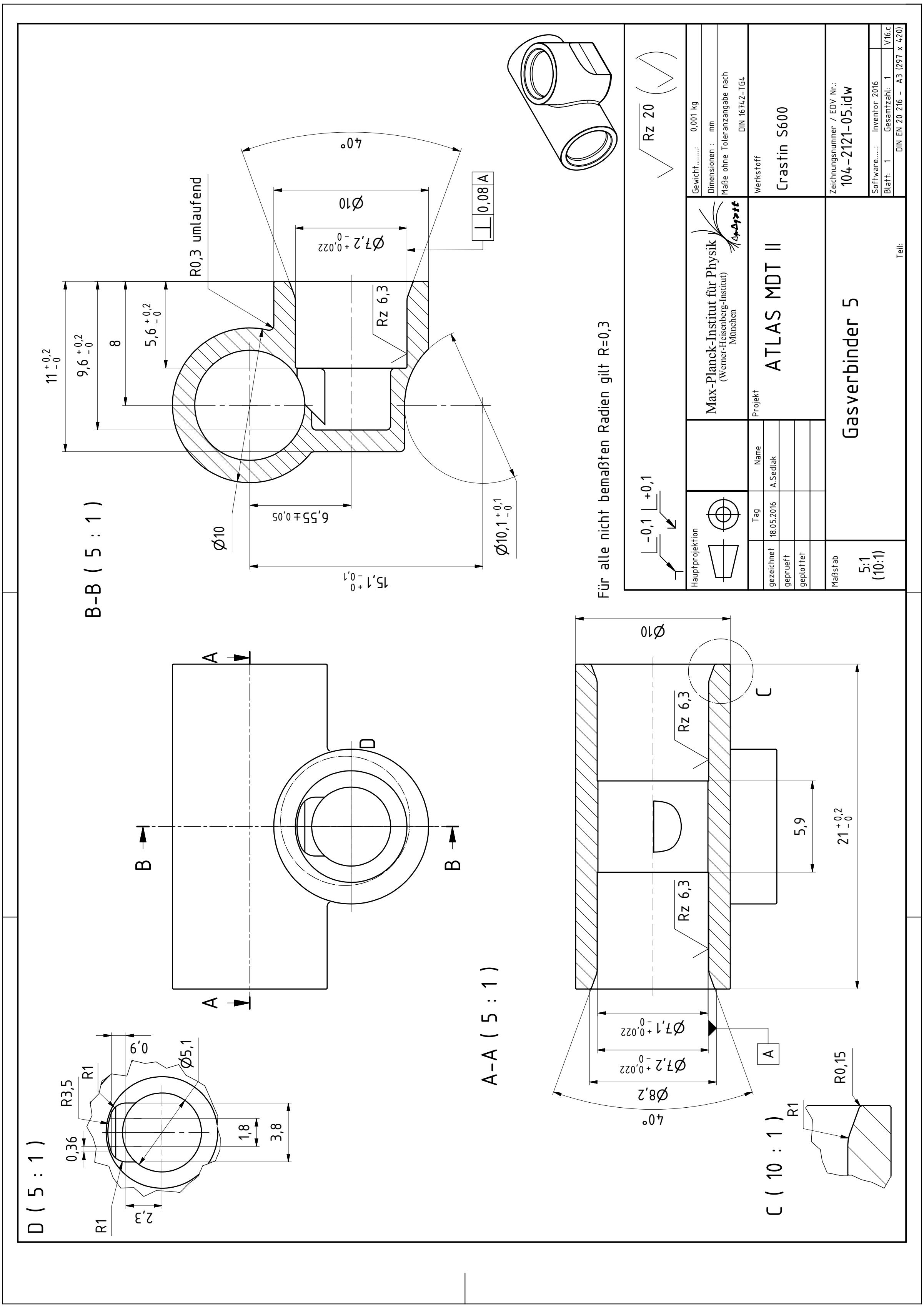

Figure 33: Schematic of fifth of eight gas distribution components stacked in groups of four to connect four tubes to gas.

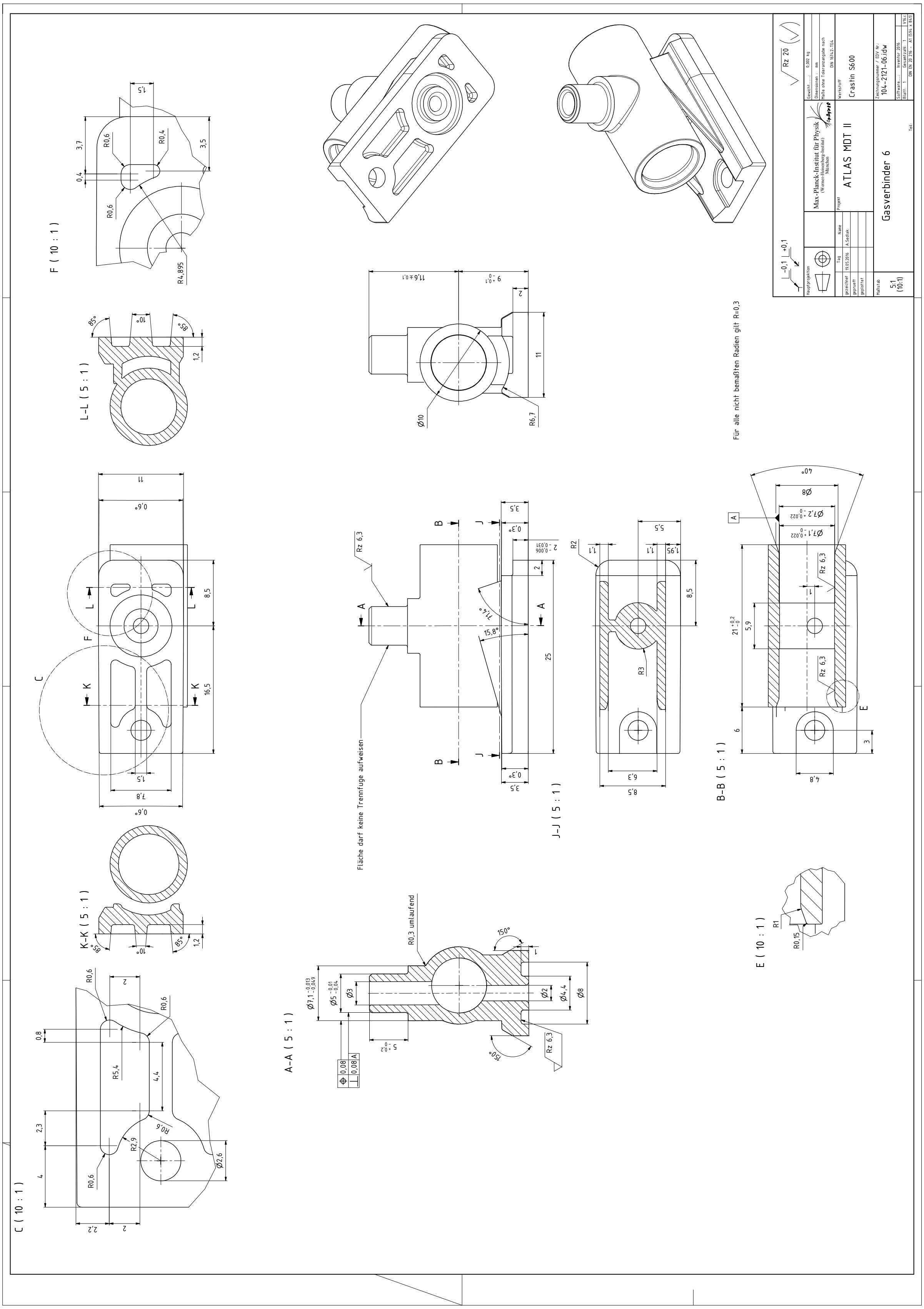

Figure 34: Schematic of sixth of eight gas distribution components stacked in groups of four to connect four tubes to gas.

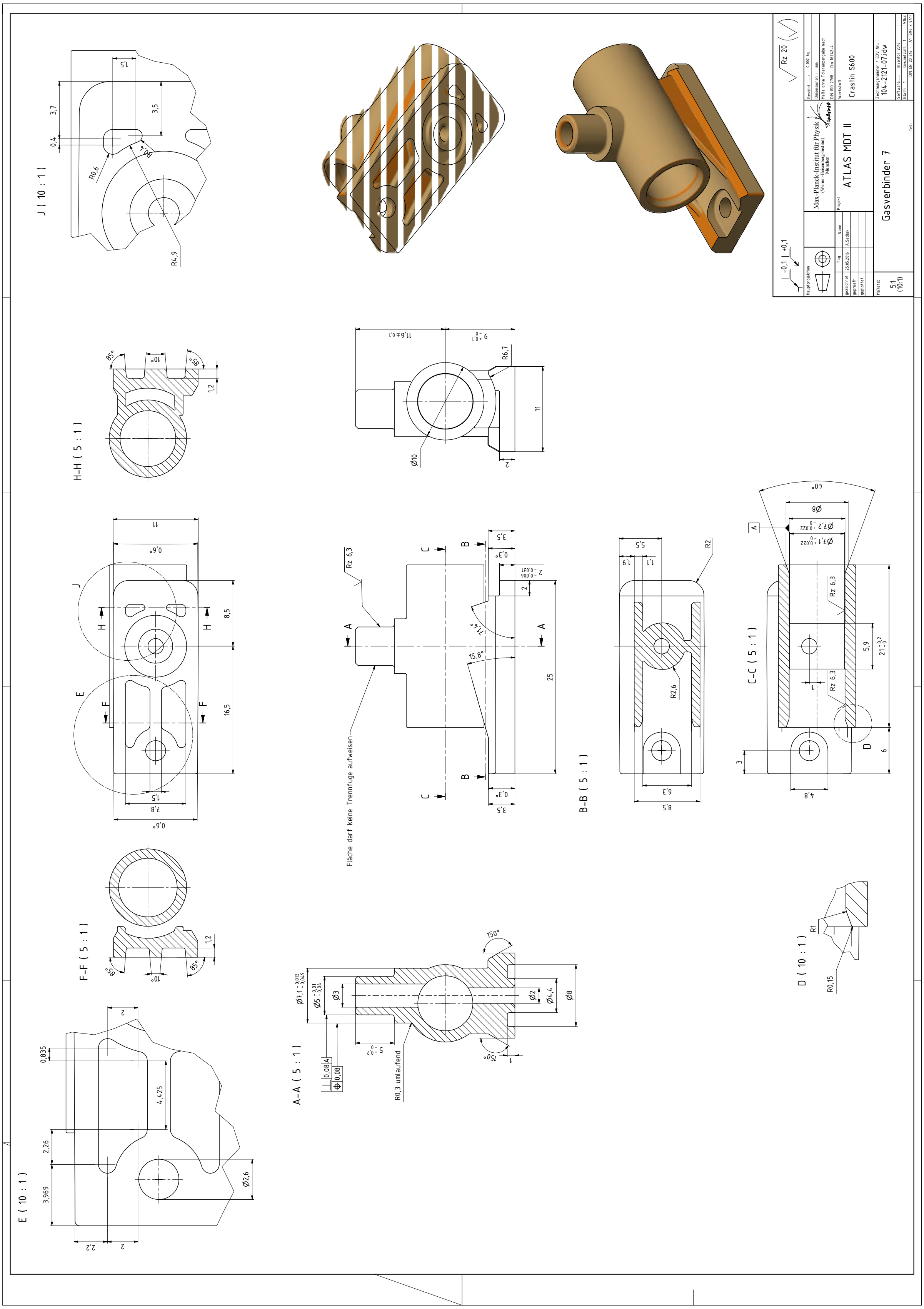

Figure 35: Schematic of seventh of eight gas distribution components stacked in groups of four to connect four tubes to gas.

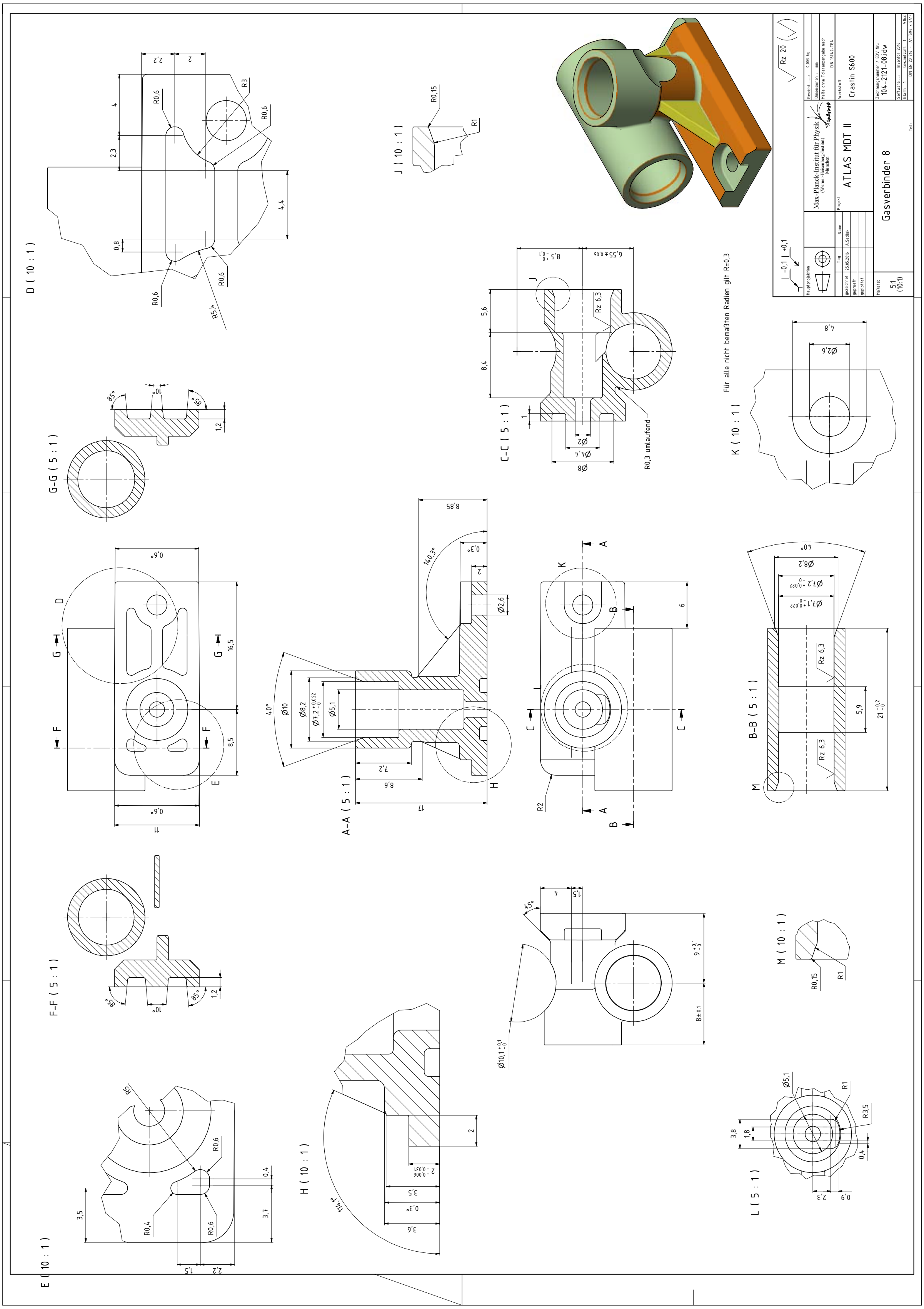

Figure 36: Schematic of eigth of eight gas distribution components stacked in groups of four to connect four tubes to gas.

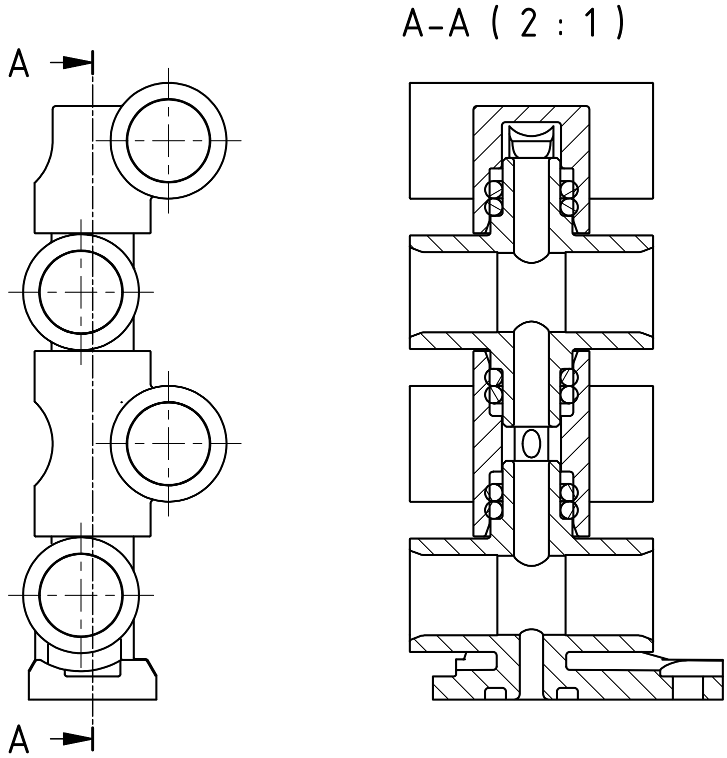

1	1	Gasverbinder 1	104-2121-01.ipt	Crastin S600
2	1	Gasverbinder 2	104-2121-02.ipt	Crastin S600
3	6	O-Ring 5x1,5	O-Ring5x1,5.ipt	EPDM
4	1	Gasverbinder 5	104-2121-05.ipt	Crastin S600
5	1	Gasverbinder 6	104-2121-06.ipt	Crastin S600
Teil	St.	Benennung	Zeichn. Nr. / EDV Nr,	Werkstoff

Stückliste

-0,1 +0,1

Hauptprojektion

Max-Planck-Institut für Physik
(Werner-Heisenberg-Institut)
München

Gewicht.........: 0,005 kg
Dimensionen : mm
Maße ohne Toleranzangabe nach
DIN ISO 2768 m K

	Tag	Name
gezeichnet	01.06.2016	A.Sedlak
geprueft		
geplottet		

Projekt
ATLAS MDT II

Werkstoff

Maßstab
2:1

Gasline Variante 1

Teil:

Zeichnungsnummer / EDV Nr.:
104-2121-00-01.idw

Software......: Inventor 2016
Blatt: 1 Gesamtzahl: 1 V16.c
DIN EN 20 216 - A4 (210 x 297)

Figure 37: First of four variants of a stack of four gas distrubtion pieces.

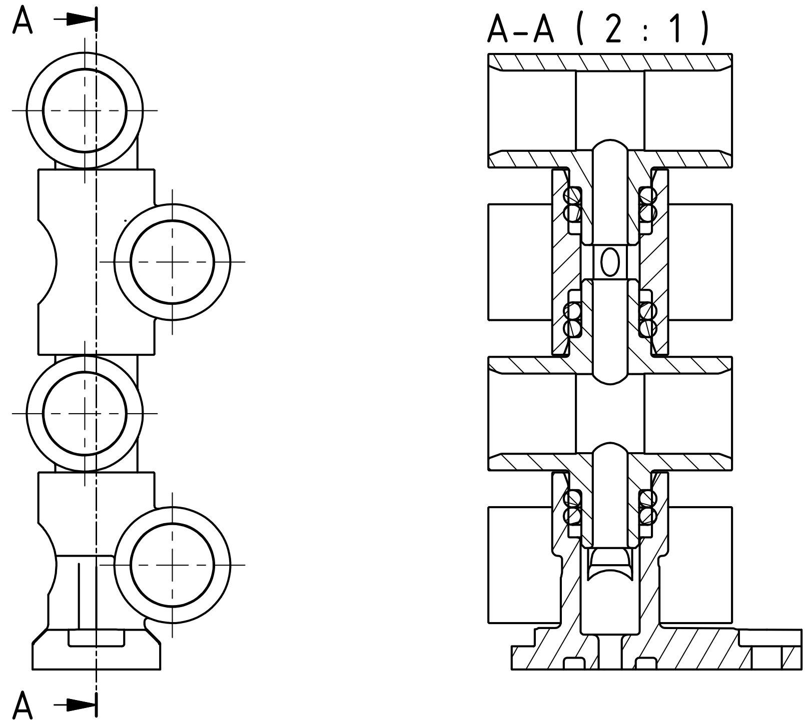

Teil	St.	Benennung	Zeichn. Nr. / EDV Nr,	Werkstoff
1	1	Gasverbinder 1	104-2121-01.ipt	Crastin S600
2	1	Gasverbinder 2	104-2121-02.ipt	Crastin S600
3	6	O-Ring 5x1,5	O-Ring5x1,5.ipt	EPDM
4	1	Gasverbinder 4	104-2121-04.ipt	Crastin S600
6	1	Gasverbinder 3	104-2121-03.ipt	Crastin S600

Stückliste

-0,1 +0,1

Hauptprojektion

Max-Planck-Institut für Physik
(Werner-Heisenberg-Institut)
München

Gewicht.........: 0,005 kg
Dimensionen : mm
Maße ohne Toleranzangabe nach DIN ISO 2768 m K

	Tag	Name
gezeichnet	01.06.2016	A.Sedlak
geprueft		
geplottet		

Projekt: ATLAS MDT II

Werkstoff

Maßstab: 2:1

Gasline Variante 2

Teil:

Zeichnungsnummer / EDV Nr.: 104-2121-00-02.idw

Software......: Inventor 2016
Blatt: 1 Gesamtzahl: 1 V16.c
DIN EN 20 216 – A4 (210 x 297)

Figure 38: Second of four variants of a stack of four gas distrubtion pieces.

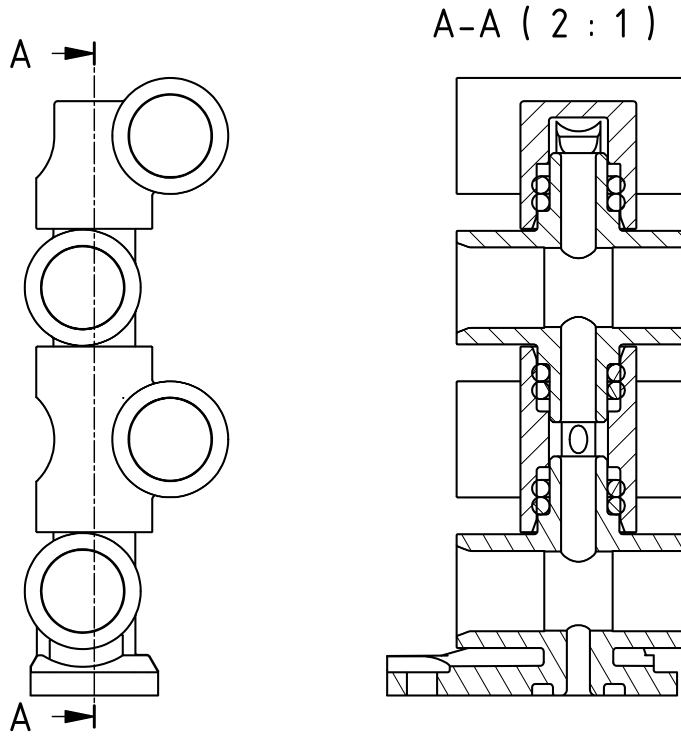

1	1	Gasverbinder 1	104-2121-01.ipt	Crastin S600
2	1	Gasverbinder 2	104-2121-02.ipt	Crastin S600
3	6	O-Ring 5x1,5	O-Ring5x1,5.ipt	EPDM
4	1	Gasverbinder 5	104-2121-05.ipt	Crastin S600
6	1	Gasverbinder 7	104-2121-07.ipt	Crastin S600
Teil	St.	Benennung	Zeichn. Nr. / EDV Nr,	Werkstoff

Stückliste

-0,1 +0,1

Hauptprojektion	Max-Planck-Institut für Physik (Werner-Heisenberg-Institut) München	Gewicht.........: 0,006 kg Dimensionen : mm Maße ohne Toleranzangabe nach DIN ISO 2768 m K

	Tag	Name
gezeichnet	17.06.2016	A.Sedlak
geprueft		
geplottet		

Projekt: ATLAS MDT II

Werkstoff

Maßstab: 2:1

Gasline Variante 3

Teil:

Zeichnungsnummer / EDV Nr.: 104-2121-00-03.idw

Software......: Inventor 2016

Blatt: 1 Gesamtzahl: 1 V16.c

DIN EN 20 216 - A4 (210 x 297)

Figure 39: Third of four variants of a stack of four gas distrubtion pieces.

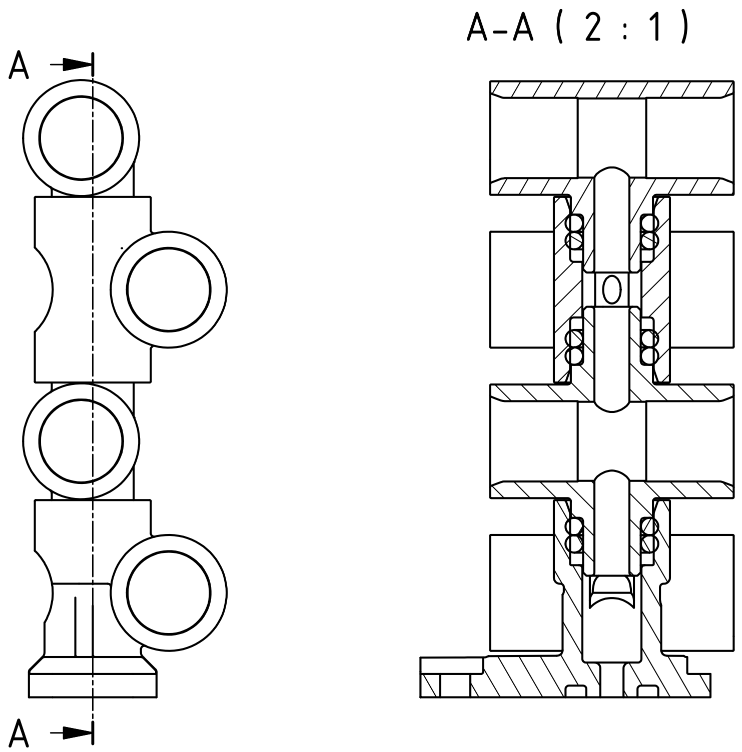

1	1	Gasverbinder 1	104-2121-01.ipt	Crastin S600
2	1	Gasverbinder 2	104-2121-02.ipt	Crastin S600
3	6	O-Ring 5x1,5	O-Ring5x1,5.ipt	EPDM
6	1	Gasverbinder 3	104-2121-03.ipt	Crastin S600
7	1	Gasverbinder 8	104-2121-08.ipt	Crastin S600
Teil	St.	Benennung	Zeichn. Nr. / EDV Nr,	Werkstoff

Stückliste

-0,1 +0,1

Hauptprojektion

Max-Planck-Institut für Physik
(Werner-Heisenberg-Institut)
München

Gewicht.........: 0,006 kg
Dimensionen : mm
Maße ohne Toleranzangabe nach DIN ISO 2768 m K

	Tag	Name
gezeichnet	17.06.2016	A.Sedlak
geprueft		
geplottet		

Projekt: ATLAS MDT II

Werkstoff

Maßstab: 2:1

Gasline Variante 4

Teil:

Zeichnungsnummer / EDV Nr.: 104-2121-00-04.idw

Software......: Inventor 2016
Blatt: 1 Gesamtzahl: 1 V16.c
DIN EN 20 216 – A4 (210 x 297)

Figure 40: Fourth of four variants of a stack of four gas distrubtion pieces.

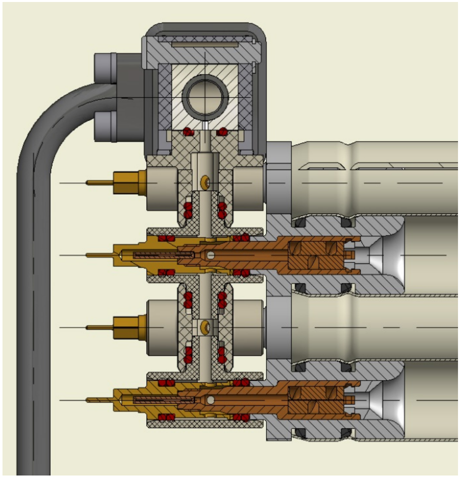

Figure 41: A side-view cutaway of the distribution of the gas over a vertical column of four tubes.

8 Cosmic Ray Testing

For each chamber, the noise and response of the electronics are tested using cosmic rays. The chamber is connected to readout electronics with an external trigger in a similar setup as what will be found in the ATLAS detector. The chamber is tested once at MPI before it is shipped to CERN. After the chamber arrives at CERN, another test is run to ensure the chamber suffered no damage during transportation before installation in the ATLAS detector.

8.1 Testing at MPI

As the sMDT chambers do not have an internal trigger, the noise and cosmic ray tests require an external trigger for the chamber. To do this, a scintillator is positioned above and below the chamber. A coincidence window of approximately 20 ns is used. A pre-mixed gas bottle, with 93% Ar, 3% CO_2, is connected, via a flow regulator, to the chamber. At the output, a pressure sensor and flow monitor is connected. The flow monitor ensures that the gas is recycled at a rate of approximately 10 l/h, and the pressure sensor ensures that the internal pressure of the chamber is the operating value (3 bar absolute). The readout from the flow monitor and pressure sensor is used to automatically adjust the flow on the intake. The chamber is then connected to a HV source. The distribution of HV is done on-chamber, but requires two inputs at 2,370 V. The chamber is then brought to operating conditions, with appropriate pressure, gas flow rate, and high voltage. The chamber is then used to read out cosmic ray hits. The readout window for the channels is approximately 1.3 μs. Two methods were employed to read out the data. The first was to use a GLIB (Gigabit Link Interface Board), which can read out a maximum of six boards at once. One readout is required for timing and triggering from the scintillators, allowing for five cards to be read out at the same time. The other method is to use the on-chamber CSM (Chamber Service Module) which can read out all 18 boards on a chamber simultaneously. However, for these tests (as was the case for the GLIB), one input slot was initially needed for triggering and timing from the scintillator. Later tests utilized a full VME crate which allowed for the readout of the maximum number of boards (6 or 18 from GLIB or CSM, respectively).

PLACEHOLDERPLACEHOLDER

Figure 42: A schematic of the Faraday cages which cover the RO and HV sides of the chamber. The bottom left shows the cages as seen from the RO side, the lower right as seen from the HV side. The top row show various additional views of the Faraday cages.

Figure 43: Chamber seen from HV side (right) and RO side (left) with gas and HV system installed.

Figure 44: Chamber with readout system installed. Note: the two gaps correspond to the cutouts required for the ATLAS alignment system. In the center are the four valves, two for gas in (left side of the chamber) and two for gas out (right side of the chamber).

Figure 45: Completed chamber with Faraday cages seen from HV side (left) and RO side (right).

8.1.1 Testing Results from MPI

The chambers were completely installed with new mezzanine cards. The setup was also modified to better reflect the final setup to be used in the ATLAS Muon Spectrometer. Firstly, the GLIB board was not used. Instead, the on-chamber CSM was used to read out the boards. Secondly, a dedicated triggering and timing board was used off chamber, allowing for all mezzanine cards to be read out simultaneously.

The chambers were then triggered using the scintillators placed above and below the chamber. An `OR` coincidence was required for the noise tests, to increase statistics, while an `AND` was used for the cosmic tests. This was done to restrict the triggering of the chamber to hits with tracks which go through the chamber. The noise tests and cosmic tests were done with nominal operating parameters, in particular the ADC threshold. The chamber was then isolated from the gas system and its pressure loss over at least 10 hours was measured to ensure that there were no large leaks in the gas structure installed on the chamber. Each multilayer is recorded separately. The target leak rate was 0.4 mbar/hr per multilayer. The results of the chamber gas leak test done at MPI are shown in Tab. 15. While the final leak rates were higher than the target, they are low enough such that data taking will be unaffected.

Table 15: Measured gas leak rates for all completed chambers as tested at MPI in mbar/h. Multiples of target ATLAS leak rate (0.4 mbar/hr per multilayer) is listed in parenthesis. BMG-2A-14 was sent to CERN before the gas leak rate was measured at MPI.

Chamber	Top Multilayer	Bottom Multilayer

A sample ADC spectrum, drift time spectrum, and hit distribution can be seen in Figs. 47 and 48. All chambers showed nominal spectra and distributions. The noise rate on the operational chambers was seen to be less than 5 kHz overall (e.g., Fig. 46). The average accidental hit rate (noise rate) for all chambers can be seen in Fig. 49. The cosmic test (Fig. 48) showed a slightly higher hit rate in the center of the chamber. This is as expected, since more tracks can be reconstructed in the center of the chamber as compared to the edges of the chamber, where particles can more easily travel outside of the chamber's readout area. All plots shown are the final tests run, i.e., after all modifications, including the addition of any conducting glue and tape.

Figure 46: Noise from a complete chamber.

Figure 47: Sample ADC spectrum (left) and TDC spectrum (right).

Figure 48: Sample hit distribution.

Figure 49: Average noise rates for each chamber tested at MPI.

Table 16: Chambers with specific tubes with high noise rates, highlighted in red, with the measured noise rates tested at MPI.

Figure 50: Diagram showing grounding of tubes in a multilayer. Red shows the location of grounding pins. Tubes which do not contact grounding pins are highlighted in blue.

Table 17: Chambers with specific tubes with high noise rates, highlighted in red, with the measured noise rates tested at MPI after edge tube grounding modification.

8.2 Testing at CERN

The completed chambers were shipped to CERN for an abbreviated test to confirm the chambers were undamaged during transport. Tests were conducted at the BB5 facility using a second, similar setup. The chambers were stacked two high, with scintillators placed above and below the chamber. A coincidence between the two scintillators was used as a trigger (either set to `OR` for noise runs or `AND` for cosmic runs as at MPI). The chamber's gas input was then connected to a vacuum pump and gas bottle with the appropriate gas mixture with a switching valve. This time, however, only a pressure sensor was connected at the output. The gas was purged from the system, using a vacuum pump. When the chamber was evacuated, it was then filled with gas until the tubes had an internal pressure of 3 bar. The noise test was run to check the accidental hit rate in the chamber. The cosmic test was then run in parallel to the gas leak test.

8.2.1 Testing Results from CERN

The noise on each chamber is checked to ensure that no noisy channels were introduced during shipment to CERN. The noise spectra are measured with the HV on (at 2,370 V) and off, as well as with five different ASD threshold levels: 103, 106, 108 (nominal), 110, and 112, which correspond to a threshold of -49 mV, -43 mV, -39 mV, -35 mV, and -31 mV, respectively. In all, ten noise runs were taken in total. These were undertaken to test the effects of the high voltage as well as the different thresholds on the noise seen on the electronics. The noise spectra of the chambers with HV on and ASD threshold set to the operational value of 108 can be seen in Tab. 18. No new noisy tubes were introduced during transport from MPI to CERN.

Then, a cosmic ray test was run overnight to ensure that the drift time spectra are still as expected, and that the response to hits throughout the chamber were still within expectations. In parallel, a gas leak test was run to ensure that no multilayer showed excessive leaking in comparison to the tests conducted at MPI. Again, this run was required to be at least 10 hours long. The cosmic ray hits spectra can be seen in Tab. 19. The red distribution in each plot corresponds to the hits associated with cosmic tracks. The distributions show the expected "bulge" in the middle, as was seen in MPI. Clearly seen in each distribution is also the cutout, which manifests as a large gap in hits in the chamber. Furthermore, there are no additional tubes which show no hits or no noise, indicating that no connections between the tubes, readout electronics, or high voltage systems were damaged during transport.

The gas leak test results are seen in Tab. 20. These also show that no significant damage was done during transport to the gas system of the chambers.

Table 18: Measured noise rates for completed chambers at CERN with HV on and the ASD threshold of 108 (or 39 mV, the operational value). As before, the left column corresponds to the upper multilayer, and the right column corresponds to the lower multilayer. The four plots in each column, from top to bottom, correspond to the four layers of tubes in each multilayer.

Chamber	

Table 19: Measured cosmic hit rates spectra for completed chambers at CERN. The total hits per tube is shown in black, and the hits associated with cosmic tracks are shown in red. As before, the left column corresponds to the upper multilayer, and the right column corresponds to the lower multilayer. The four plots in each column, from top to bottom, correspond to the four layers of tubes in each multilayer.

Chamber	

Table 20: Measured gas leak rates for all completed chambers as tested at BB5 in mbar/h. Multiples of target ATLAS leak rate (0.4 mbar/hr per multilayer) is listed in parenthesis.

Chamber	Top Multilayer	Bottom Multilayer

9 Conclusions

Testing conducted at MPI showed that tubes could be consistently constructed to within acceptable specifications: the tubes were gas-tight and sealed properly; the tubes had the proper tension on the wires; the wires did not loosen over time to unacceptable levels; and the tubes did not draw excessive current when brought to (and even above) their operating voltage. In the end,

Not reviewed, for internal circulation only

References

[1] *ATLAS muon spectrometer: Technical Design Report*, Technical Design Report ATLAS, CERN, 1997, URL: http://cds.cern.ch/record/331068.

[2] Y. Arai et al., *ATLAS Muon Drift Tube Electronics*, Journal of Instrumentation **3** (2008) P09001, URL: http://stacks.iop.org/1748-0221/3/i=09/a=P09001.

[3] Oracle Corporation, *MySQL 5.5 Reference Manual*, URL: https://downloads.mysql.com/docs/refman-5.5-en.a4.pdf.

[4] O. Korter et al., *Small-Diameter Monitored Drift Tube (sMDT) BMG Chamber Construction and Testing*.

[5] O. Korter et al., *Construction, Testing, and Installation of New sMDT Chambers for the BME Elevator-region Upgrade*.

[6] B. Bittner et al., *Development of Muon Drift-Tube Detectors for High-Luminosity Upgrades of the Large Hadron Collider*, Nucl. Instrum. Meth. **A617** (2010) 169, arXiv: 1603.09504 [physics.ins-det].

[7] H. Kroha et al., *Construction and test of a full prototype drift-tube chamber for the upgrade of the ATLAS muon spectrometer at high LHC luminosities*, Nucl. Instrum. Meth. **A718** (2013) 427.

[8] G Aielli et al., 'Proposal for the Upgrade of the Elevator Regions in the ATLAS Barrel Muon Spectrometer', tech. rep. ATL-MUON-INT-2014-001, CERN, 2014, URL: https://cds.cern.ch/record/1642793.

[9] C. Ferretti and H. Kroha, *Upgrades of the ATLAS Muon Spectrometer with sMDT Chambers*, Nucl. Instrum. Meth. **A824** (2016) 538, arXiv: 1603.09544 [physics.ins-det].

[10] H. Kroha et al., *Construction and Test of New Precision Drift-Tube Chambers for the ATLAS Muon Spectrometer*, Nucl. Instrum. Meth. **A845** (2017) 244, arXiv: 1603.08760 [physics.ins-det].

[11] H. Kroha, 'Proposal for the Improvement of the ATLAS Muon Spectrometer Momentum Resolution in Barrel Sectors 12 and 14', tech. rep. ATL-MUON-INT-2015-001, CERN, 2015, URL: https://cds.cern.ch/record/1984472.

[12] G. Aielli et al., 'The ATLAS BIS78 Project', tech. rep. ATL-COM-MUON-2016-018, CERN, 2015, URL: https://cds.cern.ch/record/2156994.

[13] M. Deile et al., *Resolution and Efficiency of the ATLAS Muon Drift-Tube Chambers at High Background Rates*, Nucl. Instrum. Meth. **A535** (2004) 212, arXiv: 1603.09572 [physics.ins-det].

[14] S. Horvat et al., *Operation of the ATLAS muon drift-tube chambers at high background rates and in magnetic fields*, IEEE Transactions on Nuclear Science **53** (2006) 562, ISSN: 0018-9499.

[15] B. Bittner, H. Kroha and O. Kortner, 'Development and Characterisation of New High-Rate Muon Drift Tube Detectors', Presented 30 Jul 2012, PhD thesis: Munich, Tech. U., 2012, URL: https://cds.cern.ch/record/1479585.

[16] P. Schwegler and H. Kroha, 'High-Rate Performance of Muon Drift Tube Detectors', Presented 14 07 2014, PhD thesis: Munich, Tech. U., 2014, URL: https://cds.cern.ch/record/1746370.

[17] B. Bittner et al., *Performance of drift-tube detectors at high counting rates for high-luminosity LHC upgrades*, Nucl. Instrum. Meth. **A732** (2013) 250, arXiv: 1603.09508 [physics.ins-det].

[18] O. Kortner et al., *Precision muon tracking detectors and read-out electronics for operation at very high background rates at future colliders*, Nucl. Instrum. Meth. **A824** (2016) 556.

[19] P. Schwegler et al., 'Optimization of the front-end electronics of Drift Tube chambers for high-rate operation', *2014 IEEE Nuclear Science Symposium and Medical Imaging Conference (NSS/MIC)*, 2014 1.

[20] S. Nowak et al., 'Optimisation of the Read-out Electronics of Muon Drift-Tube Chambers for Very High Background Rates at HL-LHC and Future Colliders', tech. rep., 2016 7581815, arXiv: 1603.08841 [physics.ins-det], URL: https://inspirehep.net/record/1436364/files/arXiv:1603.08841.pdf.

[21] J Christiansen, 'HPTDC High Performance Time to Digital Converter', tech. rep., Version 2.2 for HPTDC version 1.3: CERN, 2004, URL: https://cds.cern.ch/record/1067476.

List of contributions